2007

Numerical investigation of effect of buoyancy on the wake of a heated cylinder in contra flow

Khyati B. Varma
Iowa State University

Numerical investigation of effect of buoyancy on the wake of a heated cylinder in contra flow

by

Khyati B. Varma

A thesis submitted to the graduate faculty

in partial fulfillment of the requirements for the degree of

MASTER OF SCIENCE

Major: Aerospace Engineering

Program of Study Committee:
Z. J. Wang, Co-major Professor
H. Hu, Co-major Professor
S. C. Kong

Iowa State University

Ames, Iowa

2007

TABLE OF CONTENTS

LIST OF TABLES

LIST OF FIGURES

ACKNOWLEDGEMENTS

I would like to take this opportunity to express my deep appreciation and gratitude to my advisors Dr. Z. J. Wang and Dr. Hui Hu for their suggestion of such an interesting problem and constantly guiding me throughout this research work. Their encouragement and motivation during this study has enabled me to earn wealth of knowledge and conduct research in a fruitful manner. They have been very cooperative whenever I had trouble and helped me get a deeper insight into the physics of the problem. Without the guidance and support of my eminent advisors this master's thesis could not have been successfully completed.

I would also like to thank my research group members for their valuable suggestions and ideas. Their encouragement and friendly suggestions during the research group meetings and personal interaction motivated me to pursue my research interest successfully.

CHAPTER 1. INTRODUCTION

1.1 Overview

For over a century, the wake flow behind a cylinder has captivated the attention of scientists and engineers. Flow over a cylinder results in the vortex shedding phenomenon over a wide range of Reynolds number (*Re*) and is a well investigated bench mark problem with a vast amount of literature [1]. A number of studies focus on the wake stability and vortex shedding characteristics for an unheated cylinder for low *Re* [2]. In the last decade, researchers have worked in the field of 3D wake dynamics behind an unheated cylinder with advances in experimental and numerical studies [3, 4].

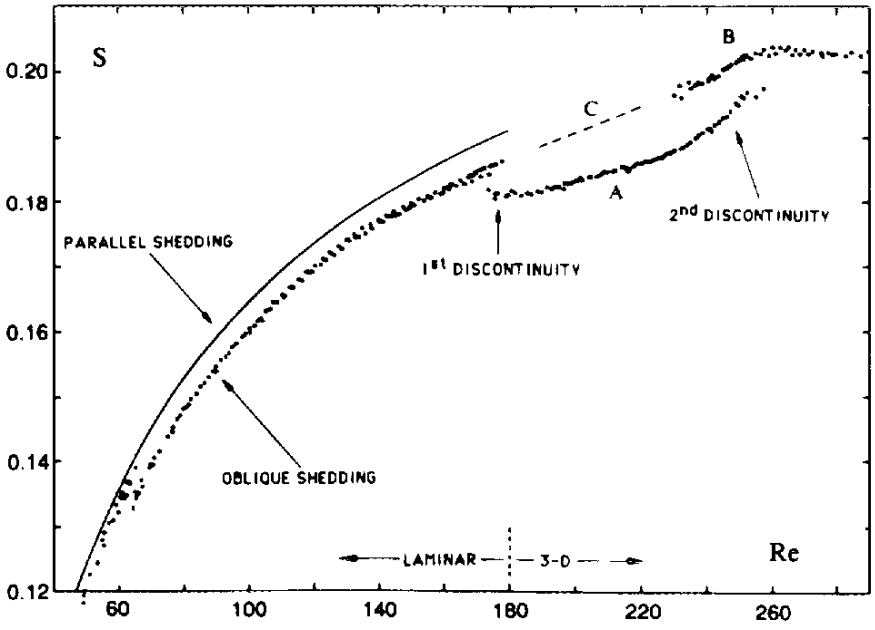

Figure 1. Strouhal-Reynolds number relationship over laminar and three-dimensional transition regimes [3]

Figure 1 illustrates the transition phenomenon as studied by Williamson [3]. Without a heat input 3D-transition takes place at around *Re*=180. The letters A, B and C refer to different three-dimensional shedding modes.

After an extensive review of the literature on wake flow behind unheated and heated cylinder, the present study aims at the numerical investigation of flow over a heated cylinder in a contra (vertically downward) flow arrangement and the effect of buoyancy on the wake behind it. The heat induced buoyancy effects are expressed by Grashof number ($Gr = g\beta(T_w - T_\infty)d^3/\nu_\infty^2$) and the relative importance of the forced and buoyant effects is indicated by Richardson number ($Ri = Re/Gr^2$). With the increasing *Ri* the heat transfer process around the heated cylinder changes from forced convection to the mixed convection regime. This is revealed in the studies by Maosheng Ren and Steehoven [5] and as schematically represented in Fig. 2.

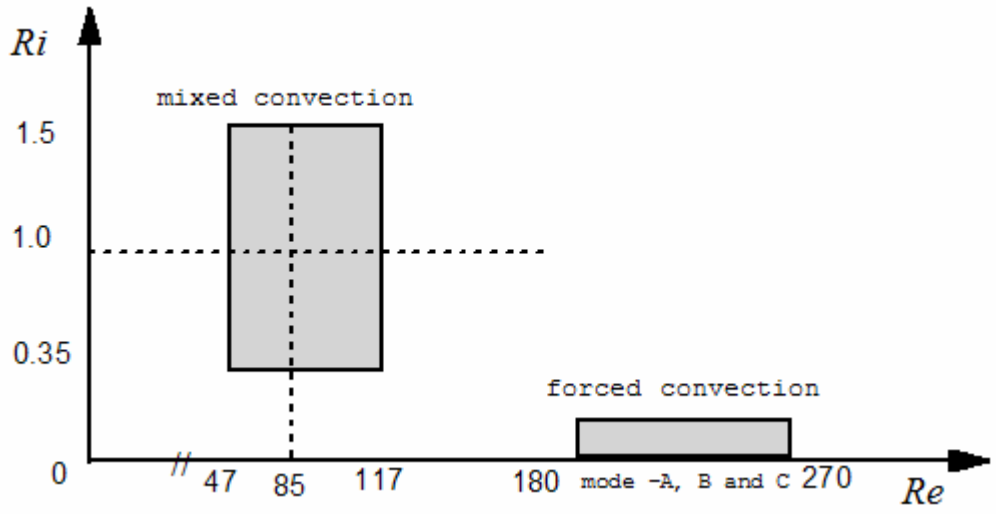

Figure 2. The three-dimensional transition as a function of Re and Ri [5].

Williamson concluded from his experiments that for an unheated cylinder, the flow becomes 3D when the *Re* is greater than 180 [3]. However the 3D behavior can be observed for even a lower *Re* if the aspect ratio (*AR*) of the cylinder evaluated as the ratio of length (*L*) of cylinder to its diameter(*d*) is low i.e. if the cylinder has a finite length. The results presented by Williamson vary for the aspect ratio less than 28 and larger aspect ratios. Same kind of behavior is observed by S. Mittal [6] and the end conditions determine the mode of vortex shedding for a finite cylinder. His

studies indicate that the wake transition regime that is known to exist on the *Re* range of 190-250 for large *AR* cylinders is either extended and/or delayed for a cylinder of small aspect-ratio with “no-slip” walls.

However the 3D transition occurring for mixed convection, denoted as mode E, is located at a much lower Re for cylinder in crossflow. The study by Maosheng Ren [5] focuses on *Re*=85 and *Ri*=1.0.

In the current study, the aspect ratio *AR*=7, is used to faithfully model the experimental conditions. For such an *AR* and *Re*, the wake transition regime is delayed which is presented here. The results for 3D transition are discussed for *Re*=130 and *Ri*=0.0 to 1.05 and results are analyzed to see how heating would affect the transition regime. Vortex shedding becomes very complicated, when the buoyant forces take over the viscous phenomenon. The knowledge of heat transfer coefficients is certainly invaluable to designers in the development of instruments using wires such as thermo-elements and hot wire anemometers. This classical and practically interesting phenomenon has its implications in other applications such as heat exchanger tubes, nuclear reactor fuel rods, chimney stack, cooling towers, offshore structures, electronics cooling etc. A number of engineering design parameters connected with fluid flow and heat transfer become important in these studies. Apart from engineering relevance, a study of these mechanisms associated with the laminar flow past cylinders, forms the first step towards the understanding of vastly more complicated phenomenon of turbulence [7].

Researchers investigated the buoyancy effects for the first time in early seventies to study the influence of the induced heat on the heat transfer coefficient [8]. This study gave remarkable results for critical *Ri* being more than 0.2 due to the influence of thermal effects for various angles between the gravity vector and the streamwise direction. Oosthuizen and Madan [9] have studied the influence of mixed

convection over a *Re* range of 100-300 with their interest in calculating the average heat transfer. Jain and Lohar [10] have pointed out an increase in the vortex shedding frequency with increasing cylinder temperature. Furthermore, studies for thermal effects on the wake by Noto et al. [11] and Badr [12] described the flow over a horizontal heated cylinder opposing the direction of gravity. The results by Noto et al. [11] indicated the effect of increasing cylinder temperature on the Strouhal Number (*St*). According to them, the Strouhal number decreases to almost zero after a critical Richardson number. The same situation was numerically analyzed by Chang and Sa [13] with detailed study on the vortex mechanisms in the near wake of a heated/cooled circular cylinder in a parallel flow (vertically upwards). With the recent development in this area, Kieft and Steehoven [14] have studied the effect of buoyancy on the heated cylinder in a horizontal cross flow. From their studies they found that the non-parallelism between the crossflow and buoyant forces cause the flow pattern to become asymmetric.

Most recently, Hu and Koochesfahani [15] have done an experimental investigation of the effect of buoyancy on the wake instability of a heated cylinder in a contra flow. So far, there is no published literature on the numerical investigation of the same problem. In the present study, special attention is given to the analysis of buoyancy effects on the wake instability of the heated cylinder in terms of vortex shedding frequency, the wake closure length, drag coefficient and the local and averaged Nusselt number of the heated cylinder.

The motivation and aim of the present study are as follows. We know that non-intrusive flow visualization experimental techniques like High Resolution Velocimetry (HiRes-PV), Laser-Induced Fluorescence (LIF), Particle Image Velocimetry (PIV) etc. turn out to be very expensive. On the other hand CFD

simulation of such a problem can give us a preliminary understanding of the flow physics at a much lower cost.

1.2 Thesis Outline

The present study aims at the numerical simulation of unsteady-state heat transfer for a laminar flow past a circular cylinder. The analysis performed focuses both, on the 3D flow transition and the wake instability due to buoyancy effects. A circular cylinder is exposed to approaching flow stream in the direction of gravity or opposing the direction of buoyant flow. The Reynolds number and the temperature (T_∞) of the incoming flow are set as *Re*=130 and $24^\circ C$ respectively. The temperature of the heated cylinder (T_w) is varied between $24^\circ C$ to $85^\circ C$ corresponding to *Ri* between 0.0 and 1.0. When T_w is same as T_∞ an isothermal wake develops behind the cylinder. However, when the cylinder temperature is higher than the flow stream temperature, a wake with buoyant force opposing the flow stream direction occurs. In addition to this, special attention is given to the influence of small aspect ratio (*AR*) and end effects on the transition mechanism due to heating.

Chapter 2 discusses the methodology involved in the present work including computational domain, mesh generation, choice and implementation of the numerical method based on the experimental set up, range of the case study and boundary conditions.

Numerical results are presented and discussed in Chapter 3. Flow visuals can be represented in the form of streamlines and vector plots in addition to analyzing pressure distribution, time averaged centerline velocities, drag coefficient and heat transfer parameters like Nusselt number (*Nu*) over the cylinder. A preliminary analysis of thermal effect of buoyancy on the 3D wake flow and transition mechanism is also done. An interesting observation about influence of small aspect

ratio and “no-slip” wall boundary conditions and end effects is also discussed. All the results are compared and validated with the experimental results of Hu and Koochesfahani [15] with some additional results.

CHAPTER 2. METHODOLOGY

2.1 Problem Definition

In the current study, numerical investigation has been conducted using a time-accurate finite-volume method solving the unsteady compressible Navier-Stokes equations. The commercial finite volume computational fluid dynamics code, FLUENT 6.0 is used for the numerical simulation. For a fixed value of Reynolds number *Re*= 130, at varying Richardson number *Ri*=0.0 to 1.0, both unsteady two-dimensional (2D) and three-dimensional (3D) flow simulations for water have been implemented trying to maintain similar characteristics of mesh generation and solver set-up to make the results comparable. The flow is assumed to be in the vertically downward direction approaching the isothermal heated copper cylinder as shown in the schematic of the problem in Fig. 3. The six cases for various temperature conditions of the heated cylinder that are studied in the present work are listed in the Table 2.1.

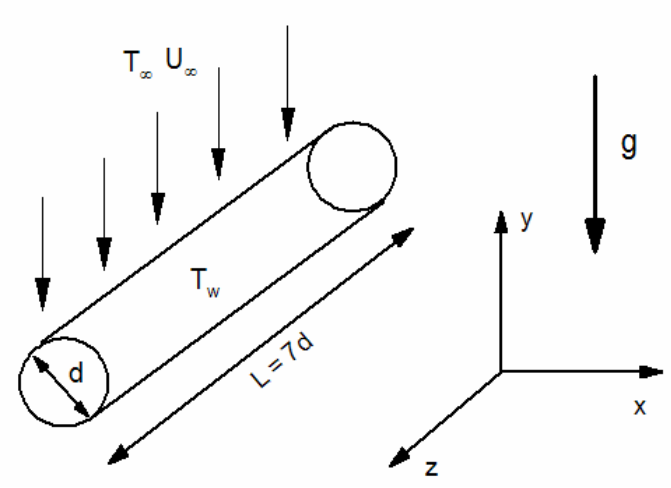

Figure 3. Schematic of approaching flow around the heated cylinder.

Table 1. The six studied cases with the controlling parameters

Case No.	T_w and T_∞	Reynolds number $\mathrm{Re} = \frac{\rho V_\infty d}{\mu_\infty}$	Grashof number $Gr = \frac{g\beta(T_w - T_\infty)d^3}{\nu_\infty^2}$	Richardson number $Ri = \frac{Gr}{\mathrm{Re}^2}$
1	T_w = 24°C, T_∞ = 24°C	130	0	0.00
2	T_w = 35°C, T_∞ = 24°C	130	3300	0.19
3	T_w = 42°C, T_∞ = 24°C	130	5400	0.31
4	T_w = 53°C, T_∞ = 24°C	130	8700	0.50
5	T_w = 66°C, T_∞ = 24°C	130	12500	0.72
6	T_w = 85°C, T_∞ = 24°C	130	18200	1.05

2.2 Computational modeling

2.2.1 Boundary Conditions

The boundary conditions for the computational domain can be specified as follows. At the inlet, uniform velocity and temperature boundary conditions were imposed. The inlet freestream velocity $V_\infty = 0.0255 m/\sec$ as calculated for $\mathrm{Re} = 130$ considering the thermophysical properties of water at temperature T_∞ =297 K or $24°C$ based on the definition of Re.

u=0, v= V_∞, T_∞ =297 K

A pressure outlet condition is specified at the outlet. With this type of boundary condition, FLUENT 6.0 uses the input pressure as the static pressure of the fluid at the outlet plane and extrapolates all other conditions from the interior of the domain.

For the lateral boundaries, the no-slip condition is applied with adiabatic thermal wall boundary condition.

u=v=w=0 and T= T_∞

The no-slip boundary condition was applied at the isothermal test cylinder where constant wall temperature condition is modeled. Based on $\mathrm{Ri} = 0.0 \text{ to } 1.0$, the temperature T_w of the copper cylinder ranges from $297K - 358K$ ($24°C - 85°C$).

u=v=w=0 and T=T_w

2.2.2 Properties of water and copper

The thermophysical properties of water vary with the temperature. The thermally induced variation of the material properties of water cannot always be safely neglected over this range of $292K - 360K$. For instance, the viscosity assumes almost 67% variation from $989 \times 10^{-6}\ Ns/m^2$ to 324×10^{-6} in the temperature range of $292K - 360K$. Hence polynomial functional relations are used to account for the temperature dependence. The equations (Eqn.1a-d) are used to determine variation with the temperature of density, specific heat, thermal conductivity and dynamic viscosity of water [12]. These formulae are implemented in the numerical computation with the user defined functions (UDFs).

$$\rho = \frac{a_0 + a_1 T + a_2 T^2 + a_3 T^3 + a_4 T^4 + a_5 T^5}{1 + a_6 T} \tag{1a}$$

$$C_p = b_0 + b_1 T + b_2 T^2 + b_3 T^3 + b_4 T^4 \tag{1b}$$

$$k = c_0 + c_1 T + c_2 T^2 + c_3 T^3 + c_4 T^4 \tag{1c}$$

$$\mu = d_0 + d_1 T + d_2 T^2 + d_3 T^3 + d_4 T^4 \tag{1d}$$

The coefficients of temperature dependence for density, specific heat, thermal conductivity and viscosity are presented in Table 2 corresponding to equations (1a-d) respectively.

Table 2. Coefficients in temperature dependence formulae

n	a_n	b_n	c_n	d_n
0	1819	1.6987	1.8231	46763
1	-12.105	-0.024932	-0.020442	-510.93
2	7.04×10^{-2}	1.469×10^{-4}	1.0365×10^{-4}	2.2991
3	-1.9675×10^{-4}	-4.3376×10^{-7}	-2.0506×10^{-7}	-4.602×10^{-3}
4	2.601×10^{-7}	6.4132×10^{-10}	1.396×10^{-10}	3.4604×10^{-6}
5	-1.3494×10^{-10}			

2.3 Numerical Method

The governing unsteady compressible Navier-Stokes equations are numerically solved using finite-volume method based CFD code FLUENT 6.0. Spatial derivatives were discretized using QUICK scheme which is based on averaging the second order upwind and central differences of a variable. The second-order implicit method was used for temporal discretization. The segregated solver was applied to solve the momentum and the energy equations and considering the difference of thermophysical properties between the fluid region and the cylinder, the double-precision solver is used. At each step, the momentum equations are first solved to obtain the velocity field. The pressure field and velocity field were coupled by PISO (Pressure Implicit with Splitting Operator) method. Upon solving the continuity and momentum equations, the energy equation was solved to achieve a quasi-steady periodic condition. The C_d was monitored over the cylinder surface as a function of time.

The steady-periodic state was assumed to be achieved when the variation in the oscillating amplitudes of the C_d was less than 1%. The convergence criterion is deemed met when the scaled residual $R^{\phi}=\dfrac{\sum_{cellsP}\left|\sum_{nb}a_{nb}\phi_{nb}+b-a_p\phi_p\right|}{\sum_{cellsP}\left|a_p\phi_p\right|}$ is less than 10^{-9} [13].

The time step size can be calculated based on the vortex shedding frequency for the unheated cylinder in terms of the Strouhal number (*St*).

$$St = \frac{f \times d}{V_\infty} \tag{2}$$

Based on the previous experimental and numerical results, we know that the *St* for flow past an unheated cylinder for *R*e=150 is approximately 0.18. In order to capture the vortex shedding correctly, we need atleast 20 to 25 time steps in one shedding cycle.

In this case, *d* =0.00476 m and V_∞ =0.0255 m/sec. Therefore, *f* =0.964 which would give the cycle time, *T*=1.0373. Hence we get the time step size $\Delta t = 1.0373/25 = 0.0415$. A thorough time refinement study is performed based on the above calculations and used consistently for all the simulations.

2.3.1 Mesh Generation

As discussed earlier, the aspect-ratio of the cylinder used for the present study is low which results in end effects due to no-slip boundary condition. This leads to a 3D transition in the wake for the present case, *Re*=130 even for the unheated case. Hence we cannot use a two-dimensional grid for our numerical simulation. However a total of over 10 two-dimensional and three-dimensional grids with varying dimensions and refinements were created. The 2D simulations were performed mainly to verify the consistency of the choices related to the computational domain dimensions and to its discretization. The computational domain is meshed using CFD-GEOM into a quadratic mesh. To obtain a structured mesh, domain decomposition in sub-volumes is needed and has been implemented as shown in the Fig. 4.

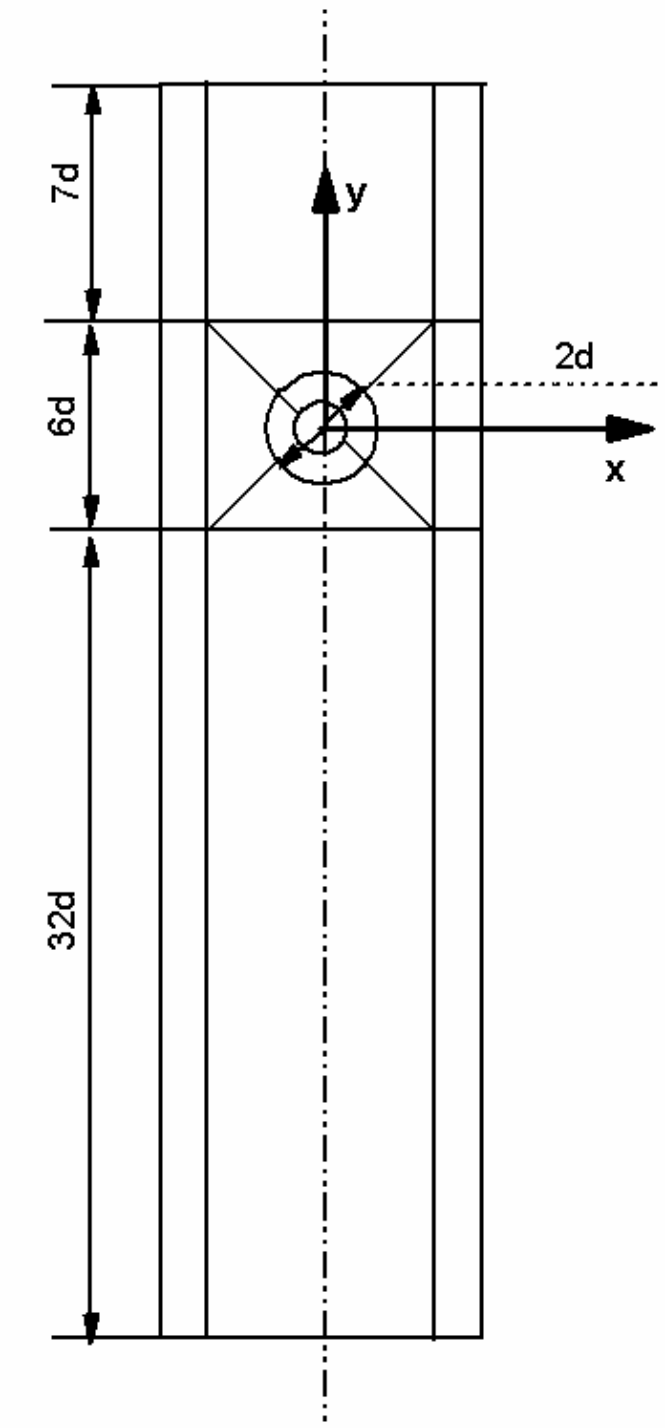

Figure 4. Domain Decomposition

In CFD models, the measurement which determines the boundary layer region is the value known as y+, which is a dimensionless number based on the

values of density, viscosity, shear stress and the distance from the wall (first cell height). Re is used to determine the y+ and is summarized for various flow conditions [13] as given in Table 3.

Table 3. Flow Regime vs Reynolds Number

Re	Flow Regime	y+/First cell height
$\mathrm{Re} < 1000$	Laminar	First Cell Height=cylinder
$1000 \le \mathrm{Re} < 20000$	Turbulent, Enhanced Wall	y+<10
$20000 > \mathrm{Re}$	Turbulent, Standard Wall	y+>30

Apart from y+ values, the various refinement factors are used to determine mesh densities shown in Table 4.

Table 4. Refinement Factor

Mesh Density	***Refinement Factor***
Coarse	1.69
Medium	1.3
Fine	1.0

Using the refinement factors and y+ values, the first cell height is calculated with the following formula.

$$First\_cell\_height = refinement\_factor \left[\frac{(y+) \times (d^{0.125} \times \mu^{0.875})}{(0.199 \times V_{\infty}{}^{0.875} \times \rho_{\infty}{}^{0.875})} \right] \quad (3)$$

Since here the *Re*=130, the flow is laminar and gives the first cell height as $2.0833 \times 10^{-2} d$ for the coarser mesh. Subsequently the first cell height for the medium and fine mesh is as shown in Table 3.

The number of intervals along each edge is determined using geometric progression and the following equation.

$$\text{Intervals=INT}\left[\frac{\log\left\{\frac{Edge\_length\times(growth\_ratio-1)}{First\_cell\_height}\right\}+1.0}{\log(growth\_ratio)}\right] \quad (4)$$

Based on the above calculations for the coarser mesh and using the domain decomposition shown in Fig. 4, the inlet and the outlet boundaries have been meshed in to 50 and 75 cells respectively. The side boundaries were meshed into 120 cells. The cylinder has been meshed using 120 cells along the circumferential direction. Thirty layers of quadratic meshes were attached inside the boundary layer with the first cell height $2.0833\times10^{-2}d$ and a growth factor of 1.25 in the radial direction.

Accuracy of CFD solutions strongly depends on the grid system which must be constructed to minimize the grid-induced errors and to resolve the flow physics accurately. For this purpose a final grid system is employed (32391 cells) after generating solutions on three different grid systems illustrated in the Table 5. The result of the assessment of this grid independence study is represented in Table 5, for the predicted values of the vortex shedding frequency of Strouhal Number. The correct reproduction of the St for the unheated cylinder is achieved indicating grid independence until the variations in the St were less than 2.0% which compares fairly well with the experimental results. Table 5 demonstrates that the fine grid yields the most grid independent result based on the criteria for St.

Table 5. Grid convergence using Strouhal number

Mesh	First Cell Height	No. of Cells	St
Coarse	$2.0833\times10^{-2}d$	13249	0.17781
Medium	$1.6026\times10^{-2}d$	22224	0.17423
Fine	$1.2327\times10^{-2}d$	32391	0.17116

Every solution present in this work is made grid independent in the manner described above. The fine grid system consists of 200 cells in the circumferential direction and 50 layers in the radial direction with the first cell height as $1.2327 \times 10^{-2} d$. The growth factor used is 1.2. An example of the fine mesh is shown in Fig. 5.

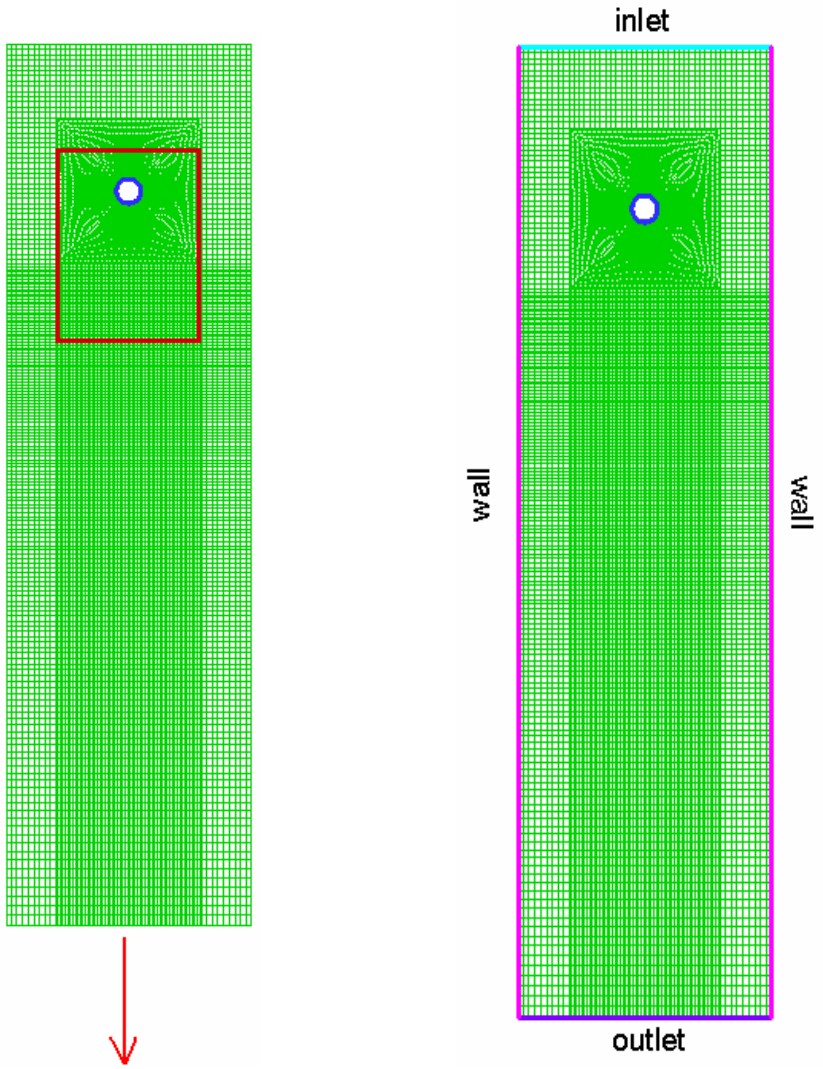

Figure 5. Fine two dimensional grid system

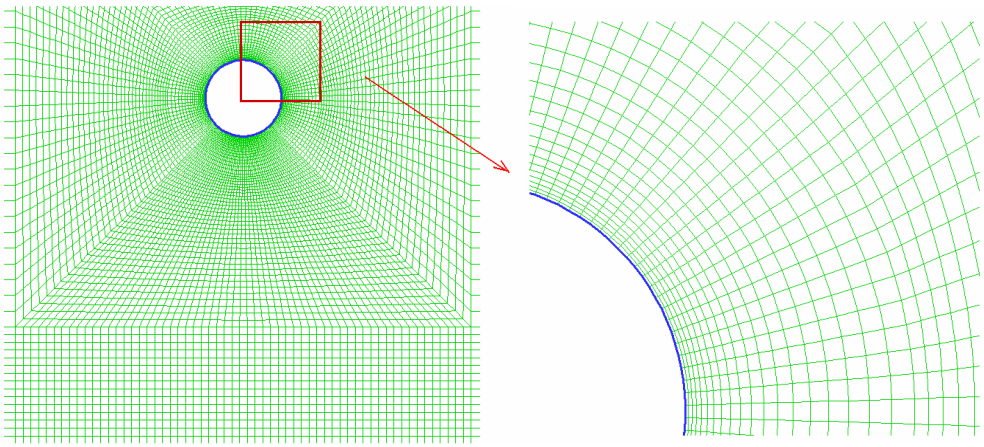

(c) (d)

Figure 5. (Continued)

As mentioned in the earlier section, 2D numerical results remain far from the physical phenomenon when the cylinder has a finite length or the aspect-ratio is low. This conclusion is clearly evident in Fig. 7 in the following chapter since 3D modes arise in the cylinder wake even for Ri=0.0 and are extended for higher Ri. The assessment of this result is demonstrated in detail in the results for Strouhal number and mean velocity profiles for 2D simulations for both unheated and heated cases.

The mesh generation for the 3D model is a clear extension of the 2D one. The length of the cylinder is about 7d to model the experimental settings in Hu et al. [15]. 40 cells with a growth ratio of 1.21 in the spanwise direction lead to a total amount of 895640 for the finest grid system. The possibility of extruding the superficial mesh in the spanwise direction allows the use of wall boundary condition for the lateral walls. Also assuming that the flow is symmetric about the center plane (transverse plane), in the spanwise direction (z-direction), a symmetry boundary condition can be used for the center plane. This reduces the total number of cells and in turn the computational time by half. Hence the 40 cells in the spanwise direction are for half the length of the cylinder. The domain decomposition for the 3D model is as shown in Fig. 6.

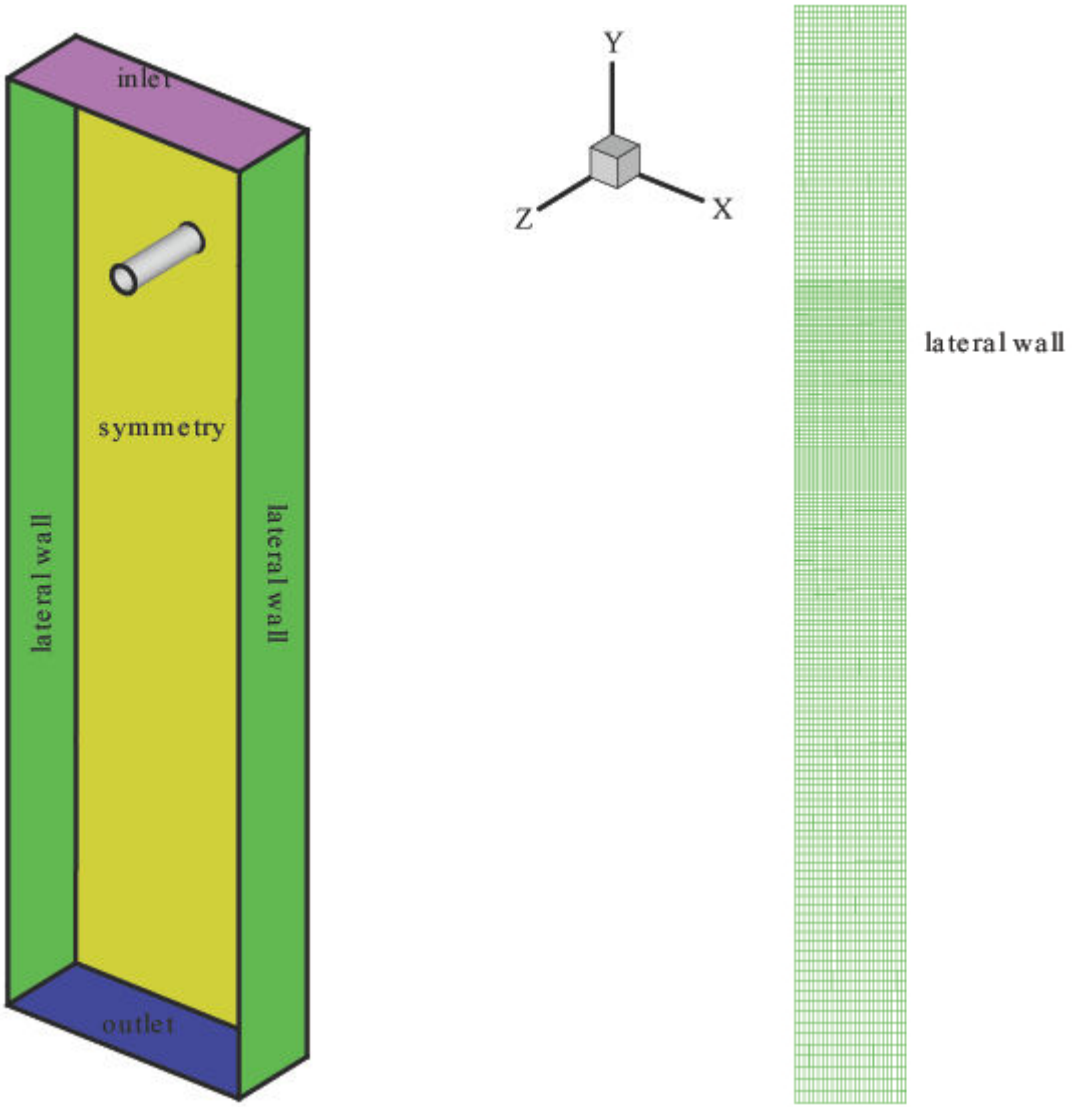

Figure 6. 3D grid system

2.3.2 2D numerical simulations

2D simulations help us to analyze the influence of the domain size and grid resolution. It has also highlighted that to obtain accurate vortex shedding frequency; a fine circumferential discretization is needed even for the unheated case. All the meshes both for 2D and 3D models are structured with quadratic and hexagonal cells respectively. The choice is tied to the need of using higher order numerical schemes available in FLUENT, only for such type of grids.

Table 6. 2D Simulation settings

Settings	Choice
Simulation	2D
Solver	Segregated implicit, Unsteady, Laminar
Temporal Discretization	Second order
Pressure	Second order
Momentum equation	Second order
Pressure-Velocity coupling	PISO
Energy equation	Second order
Inlet boundary condition	Velocity Inlet
Outlet boundary condition	Pressure outlet
Lateral wall boundary condition	Wall
Total cells amount	32391(fine mesh)

It will be discussed later in the results section that the wake behavior is no more 2D in nature if the *AR* is low. This makes the results obtained from the 2D simulations difficult to interpret and validate. This is discussed in detail in the following section and supported by the results obtained for 3D simulations.

2.3.3 3D numerical simulations

The 3D numerical settings are as represented in the Table 7. As described earlier, the 3D model is an extension of the 2D model with all the solver settings and spatial and temporal discretization consistent with the 2D simulation settings.

Table 7. 3D simulation settings

Settings	Choice
Simulation	3D
Solver	Segregated Implicit, Unsteady, Laminar
Temporal Discretization	Second order
Pressure	Second order
Momentum equation	Second order
Pressure-Velocity coupling	PISO
Energy	Second order
Inlet boundary condition	Velocity Inlet
Outlet boundary condition	Pressure outlet
Lateral wall boundary condition	Wall
Centerplane boundary condition	Symmetry
Total cells amount	689164

In the following sections the results for both 2D and 3D simulations are discussed.

CHAPTER 3. RESULTS AND DISCUSSION

3.1 Streamlines and Contours

Streamlines indicate the flow pattern at a given instant of time. The influence of buoyancy on the fluid flow in the wake region is shown by plotting the instantaneous streamlines shown in Fig. 7 for *Ri*=0.00 and in Fig. 10 for *Ri*=1.05. Here the separation angle θ_{sep}, measured from the forward stagnation point is the highest for *Ri*=0.0. The wake region is marked by a zone of reverse flow very near the cylinder surface, which can be seen in form of negative streamwise velocity vectors (Fig. 9), due to the existence of the recirculation zone downstream of the cylinder (Fig. 8). With the increasing temperature of the cylinder (*Ri*), the separation angle θ_{sep}, decreases since the direction of the flow and buoyancy oppose each other. This results in a wider wake and the recirculation zone for heated cylinder case becomes longer than the unheated cylinder.

This is also demonstrated in Fig. 10 which clearly shows that the separation angle is bigger when the cylinder is unheated, *Ri*=0.00. When we heat the cylinder (*Ri*=1.05), we see a strong upward buoyant force indicated in (Fig. 11) which results in smaller separation angle θ_{sep} seen in (Fig. 10) or early separation and the recirculation zone is pushed further downstream (Fig. 12). This also results in a wider and longer wake.

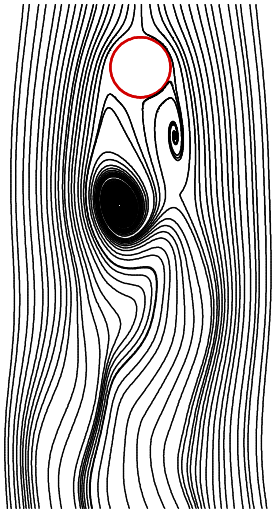

Figure 7. Streamlines for Ri=0.0

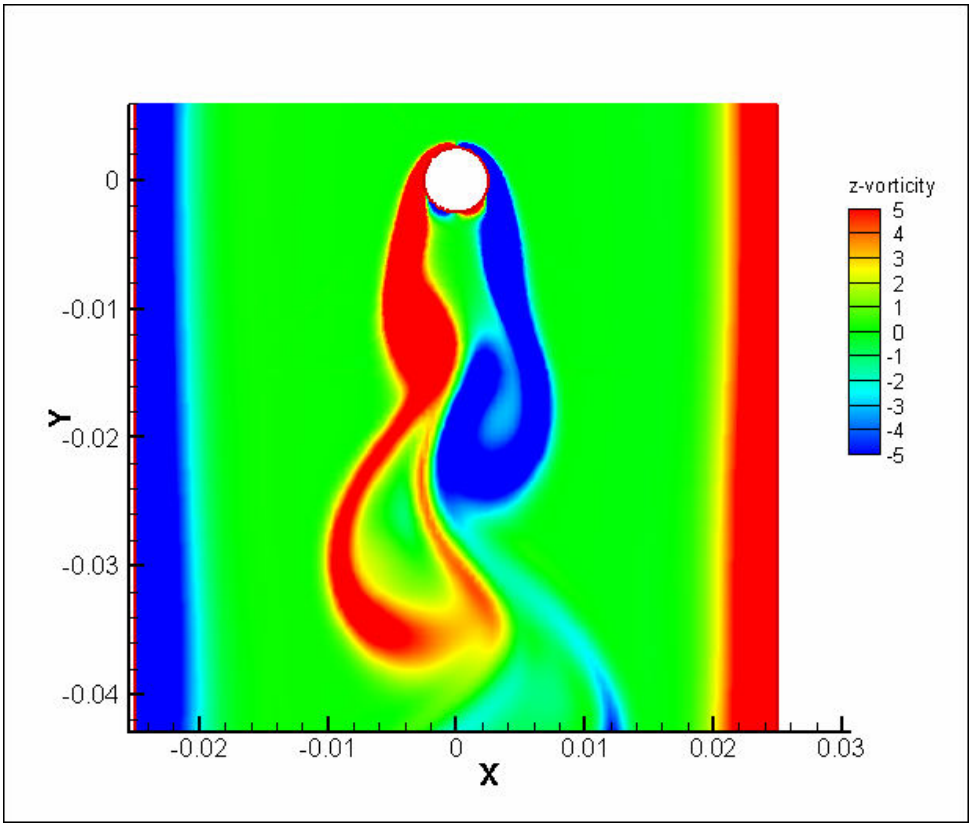

Figure 8. z-Vorticity contours Ri=0.0

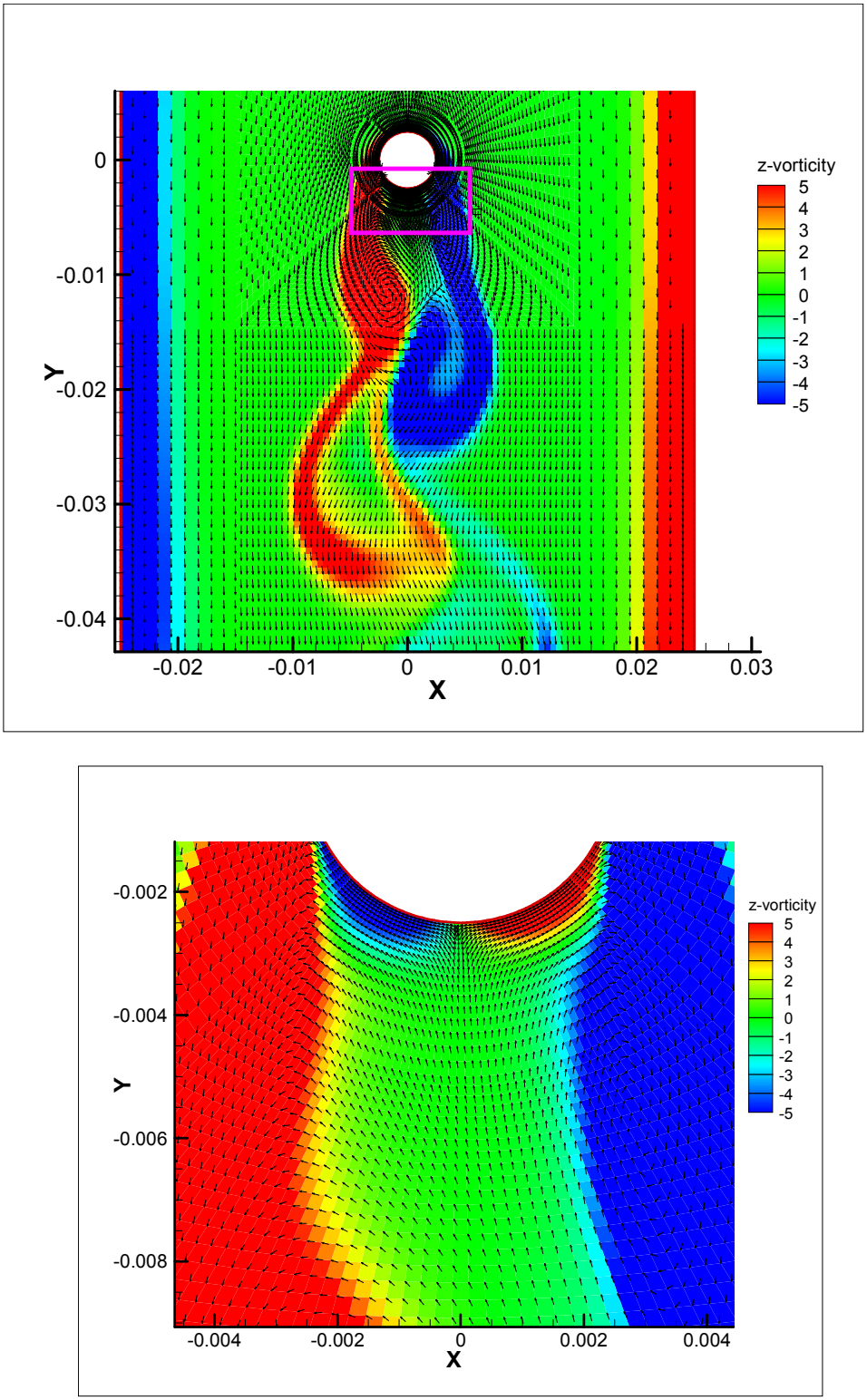

Figure 9. Vector plot for Ri=0.0 with z-vorticity contours

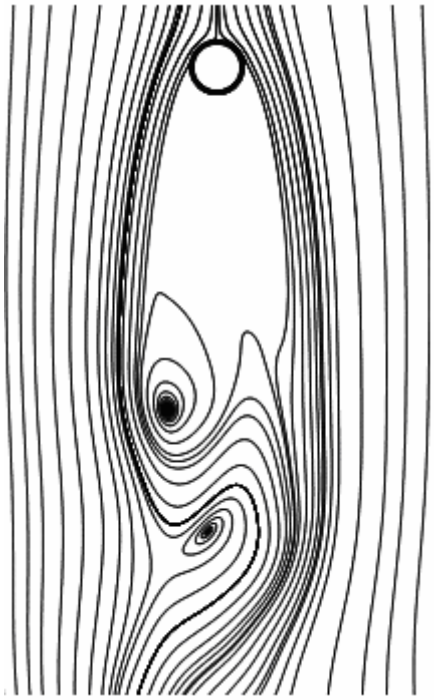

Figure 10. Streamlines Ri=1.05

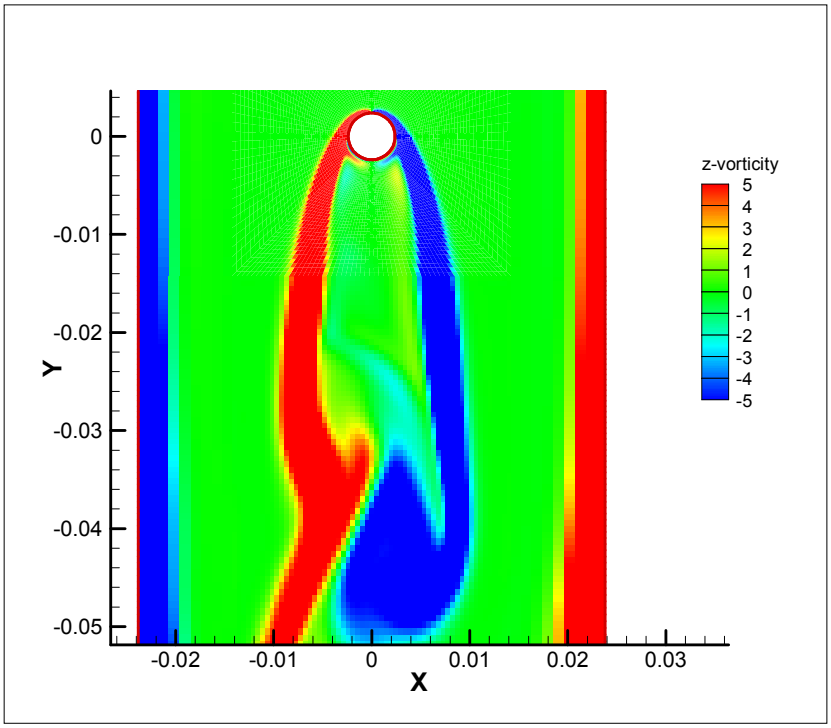

Figure 11. z-Vorticity contours Ri=1.05

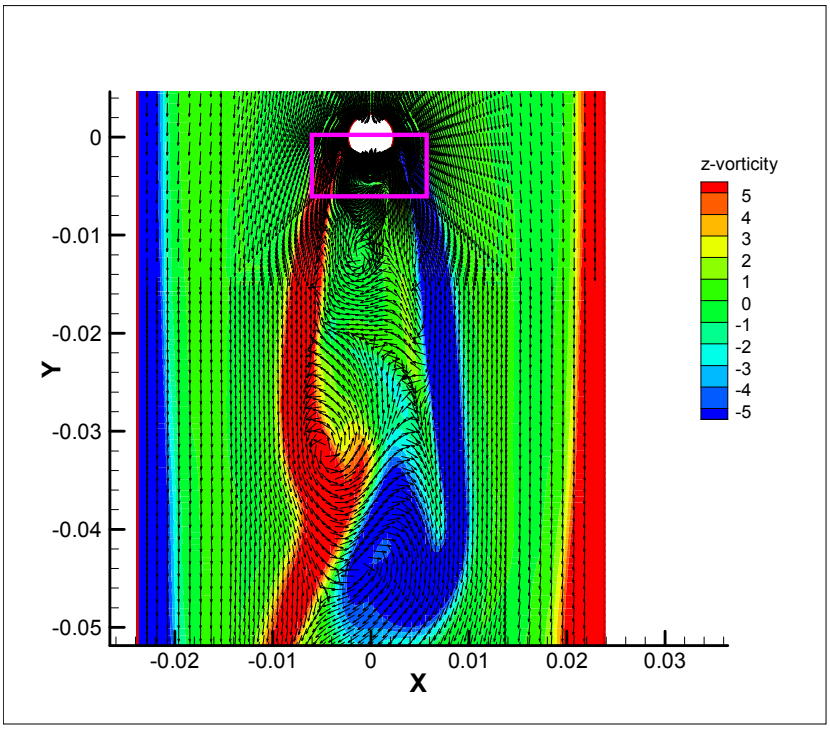

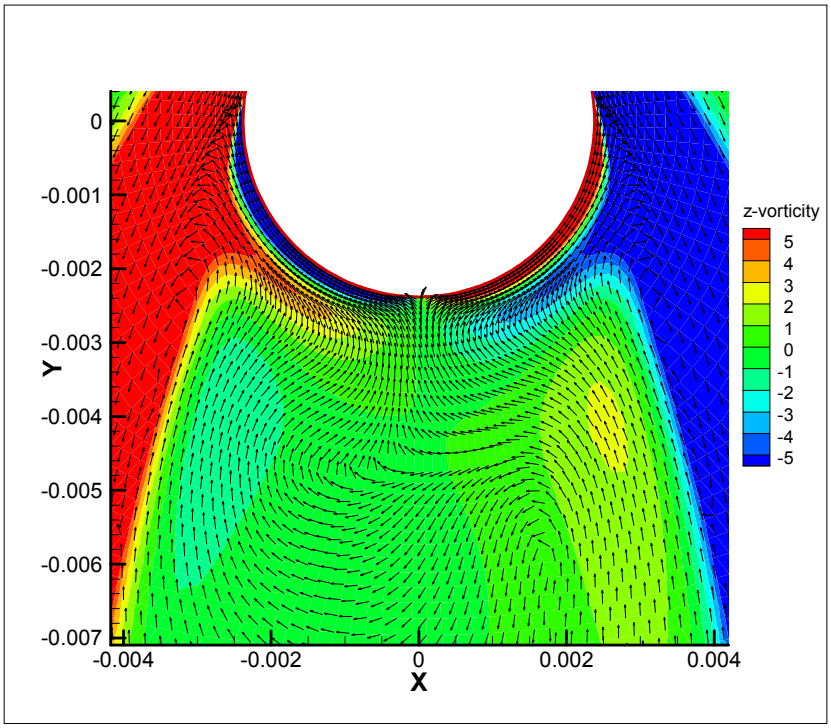

Figure 12. Vector plot for Ri=1.05 with z-vorticity contours

The near wake patterns, thus obtained can be seen in Fig. 12. As can be observed, the vortex shedding pattern for the unheated cylinder (*Ri*=0.0) is severely altered by the buoyant force. The vortex shedding is suppressed by the opposing buoyancy for *Ri*=0.30 to *Ri*=1.05.

3.2 Time-averaged wake centerline velocities

Numerical results for the time-averaged mean center line velocities along the vertical axis of the cylinder in the wake region on the symmetry plane are shown in Fig.9, for *Ri*=0.00, 0.72 and 1.05. The experimental observations of Hu [15] are also presented for the purpose of comparison.

As discussed in the previous sections, the wake region is marked by a zone of reversed flow very near the cylinder surface. It can be seen in the form of negative velocity values due to the existence of the recirculation zone downstream of the cylinder. But the wake behavior strongly depends on the end conditions in the spanwise direction. If we have a no-slip wall boundary condition as our end conditions for cylinders with low *AR*, it is certain to see 3D wake behavior even for low Reynolds number (Re<180) as mentioned earlier by Mittal [6].

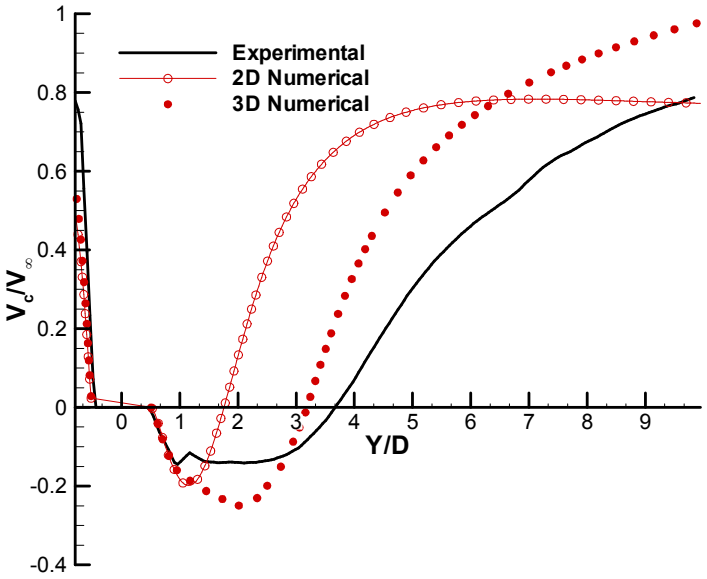

Figure 13. Comparison of time-averaged centerline velocities for Ri=0.0

This is also clearly represented in Fig. 13, which shows the time-averaged wake centerline velocities for 2D numerical simulation comparing it to the experimental data and 3D numerical results. This comparison clearly shows that the 2D simulation is unable to capture the flow phenomenon accurately.

For the unheated cylinder case, *Ri*=0.00, the velocity deficit is found to recover gradually with the increasing downstream distance around *X/D*>3 as expected [15]. With the increasing Richardson number, the stronger influence of buoyancy results in a stronger reversing flow near the trailing end of the cylinder shown in Fig. 12. Consequently the strong recirculation zone is pushed further downstream and the recovery rate of the streamwise velocity deficit decreases as also seen in Fig. 11.

This can be explained better by the time-averaged wake centerline velocities. The trend for the time-averaged centerline velocities from the present calculations is in good agreement with the experimental observations. According to the definition

given by Hu [15], wake closure length *lc* is the distance from the rear end of the heated cylinder to the point where the time-averaged mean velocity becomes zero and changes its direction. The wake closure length for unheated cylinder from the present result differs from the experimental result by almost 13%. Whereas for the heated cases of *Ri*=0.72 and *Ri*=1.05 the numerical result matches well within 10% error when compared to the experimental results.

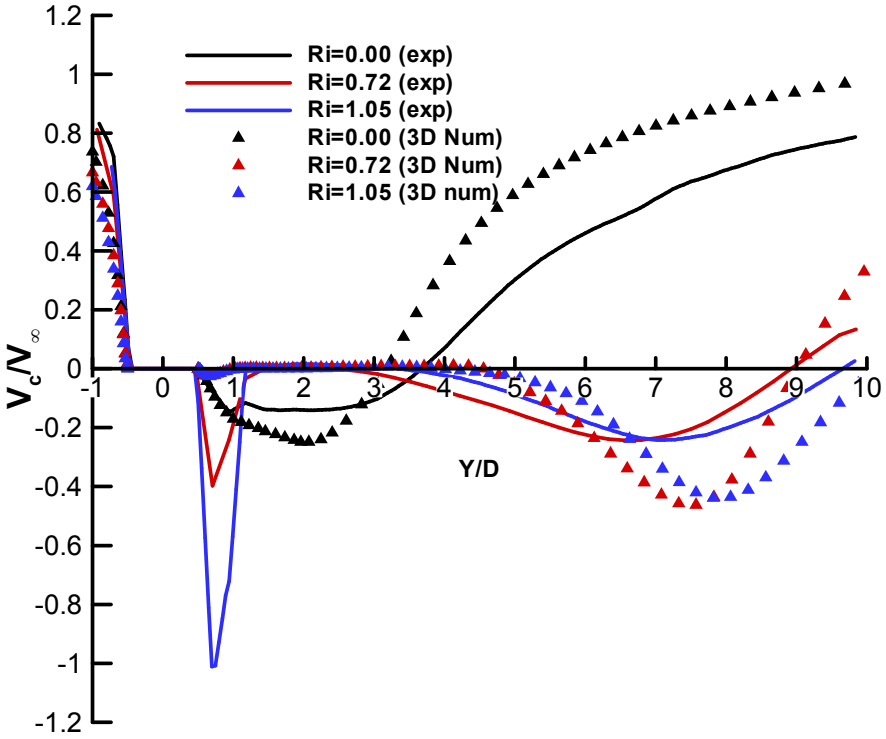

Figure 14. Time-averaged wake centerline velocities for various Ri

When the negative streamwise velocity for the present study is compared with that of the experimental results, there is a huge difference. One of the possible reasons could be that the *Re* calculation in the experiments was based on the velocity measured after the flow is fully developed where as in the present study the

Re is calculated based on the uniform velocity at the inlet. In the experiments the velocity is measured 8*d* upstream of the cylinder. The inflow length for the experiments is 25 diameters and it is certain to observe a fully developed flow for such a length. In addition to this, there is a velocity profile developed in the spanwise direction too since the aspect ratio *L/d*, is very large. It is very difficult to model such a 3D velocity profile as the inlet condition for the numerical simulation. This could also be the explanation for the variation in the wake closure length for both the unheated and heated cylinder cases.

3.3 Pressure Distribution and Time-averaged Drag Coefficient

The pressure distribution over the cylinder is shown in Fig. 15, for *Ri*=0.0, *Ri*=0.5 and *Ri*=1.05. It is known that the total drag comprises of drag due to the skin friction and pressure drop. As the temperature increases, the influence of buoyancy increases. Hence the drag due to the skin friction decreases marginally owing to the decreasing viscosity of the surrounding fluid while the drag due to the pressure drop increases substantially. Thus the drag due to skin friction can be neglected for higher *Ri* cases for the heated cylinder and pressure drag becomes dominant in the total drag calculation. The mean pressure drag is calculated as

$$\overline{D} \cong \int \overline{p} dA \tag{3}$$

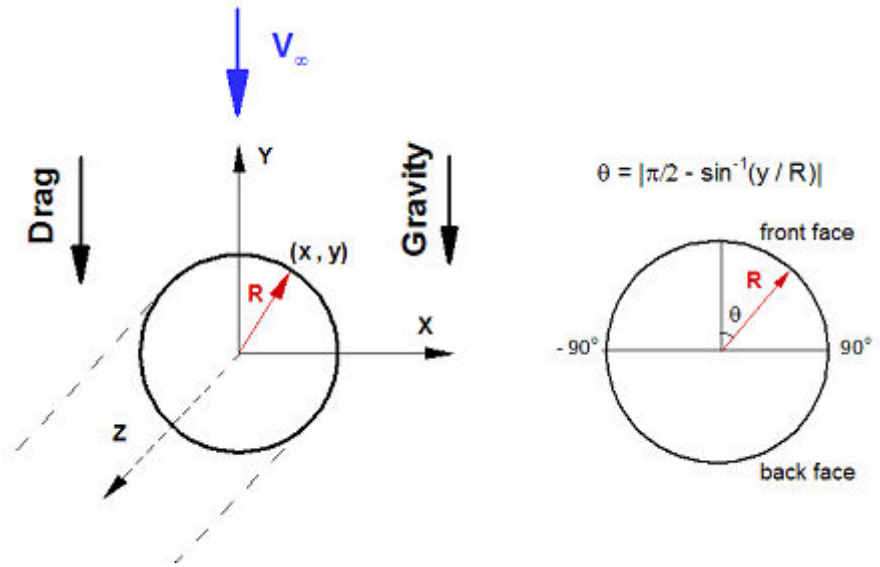

Figure 15. Schematic of pressure distribution over the cylinder

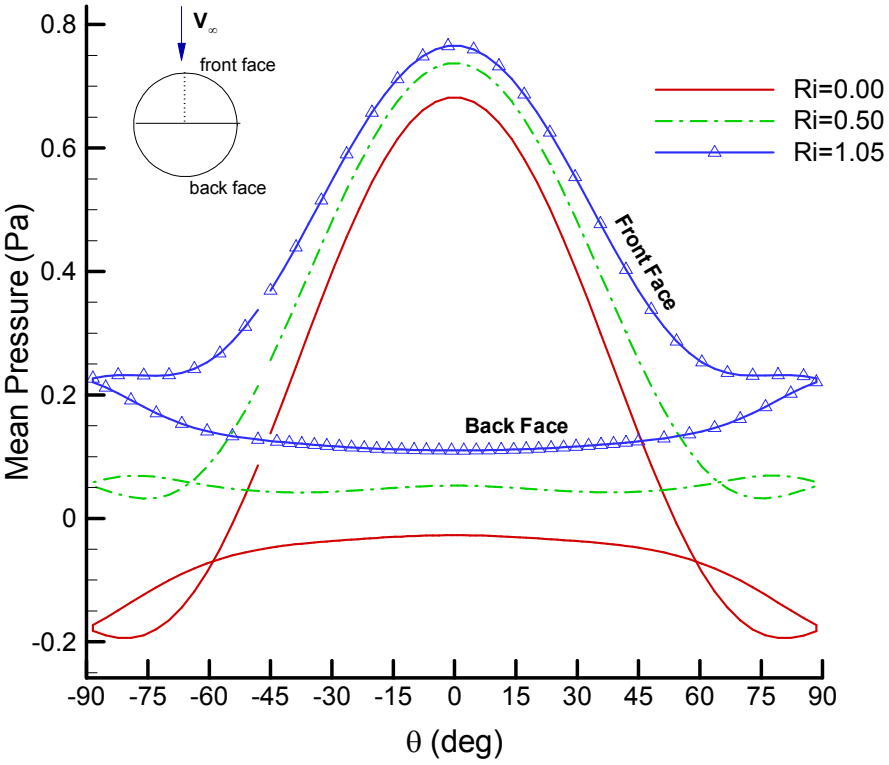

Figure 16. Mean Pressure distribution over the cylinder

Figure 17 clearly represents that the $\overline{D}$ increases as Ri increases. Due to the increasing effect of buoyancy with higher temperature of the cylinder the separation point moves towards the upstream of the heated cylinder for Ri>0.3 which is depicted in Fig.17. This flow separation results in a wider wake for the heated cylinder than the unheated cylinder. Consequently the drag is higher when the cylinder is heated than when it is unheated, due to higher contribution from the form drag. The drag coefficient C_d is averaged over a number of vortex shedding cycles to obtain $\overline{C_d}$ since the $\overline{D}$ is also averaged.

$$\overline{C_d} = \frac{2D}{\rho_\infty V_\infty{}^2 A} \tag{4}$$

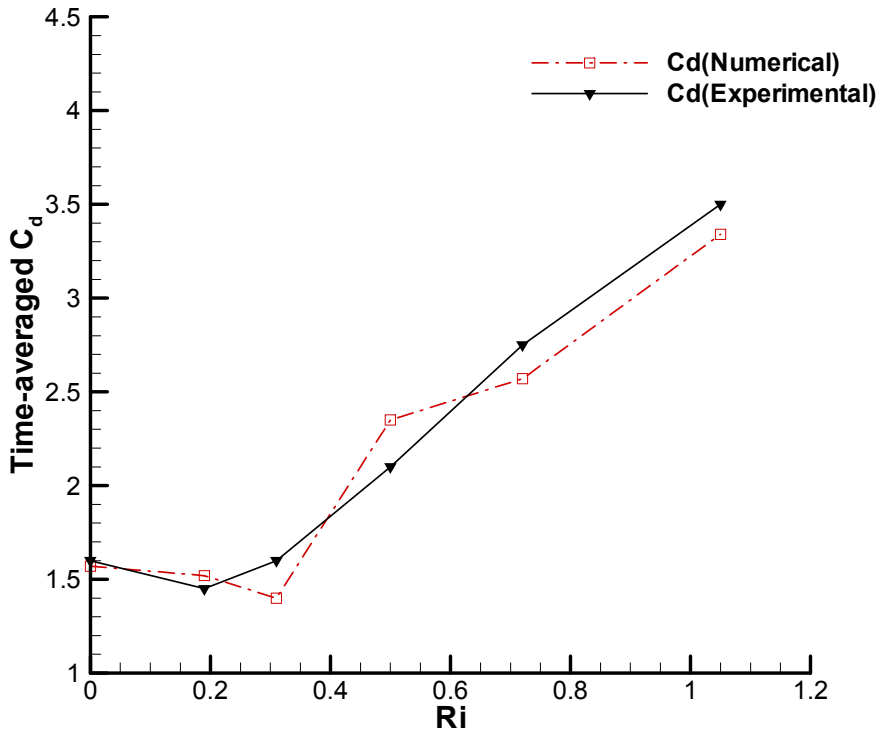

Figure 17. Time-averaged Drag Coefficient $\overline{C_d}$ as a function of Ri

It is observed in Fig.17 that the $\overline{C_d}$ for Ri=0.3 is much lower than Ri=0.0. This is explained by Hu and it is because the effect of buoyancy being is still weak[15]. But as discussed earlier for Ri>0.3 the effect of buoyancy becomes considerable which significantly influences the drag coefficient. As seen in the Fig.17, the numerical result for Ri=0.50 seems to over predict the $\overline{C_d}$ by almost 15%. This could mean that the critical Ri at which the buoyancy effects become significant would be between 0.3 and 0.5. For Ri=0.72 and Ri=1.05 it under predicts the C_d by 11.25% and 10% respectively.

3.4 Vortex Shedding Frequency

The phenomenon of vortex shedding from the bluff bodies has been studied since the pioneering work of Von Karman and Strouhal. The Strouhal Number is the measure of the oscillating fluid flow phenomenon in the wake region, and defined using the flow parameters by the following relation:

$$St = \frac{f \times d}{V_\infty}$$

where *f* is the vortex shedding frequency, d is the diameter of the cylinder and V_∞ is the free steam velocity. In the present study the Strouhal number, *St* for the six varied cases is deduced from the signal traces (Fig.18) of the temporal lift force coefficient. Figure 19 shows the spectral analysis obtained by the Fast Fourier Transform (FFT) of the lift coefficient for Re=130 and Ri=0.0.

Strouhal number obtained from the present analysis is compared with some of the existing experimental and numerical investigations for Re=100 and Ri=0.0 in Table 8. A good agreement can be noticed with the studies listed in this table. Thus for flow over an unheated cylinder the 2D simulations produce good accuracy in terms of vortex shedding frequency.

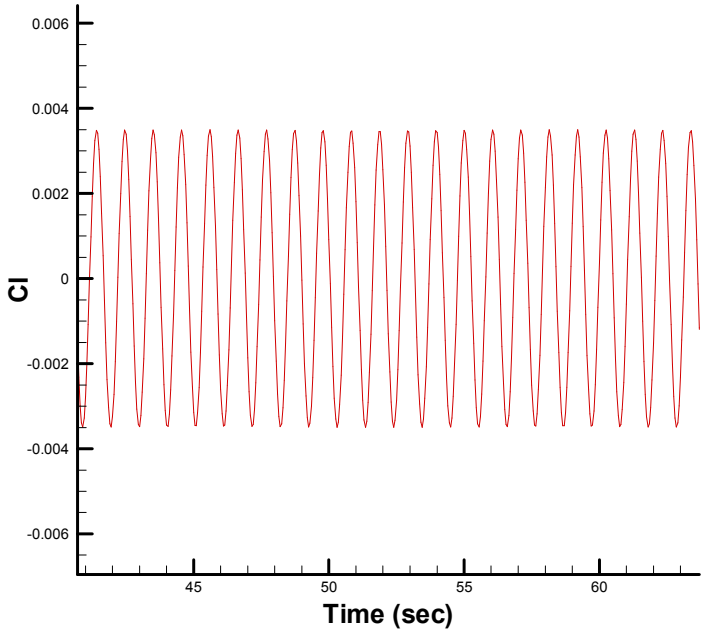

Figure 18. Temporal lift coefficient history (Ri=0.00)

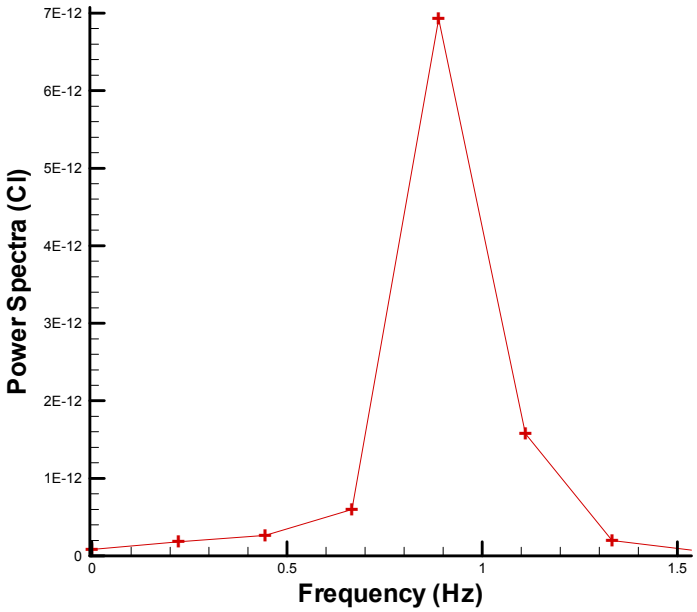

Figure 19. Spectral Analysis of Lift Convergence (Ri=0.00)

Table 8. Comparison of St at Ri=0.0

Re	Researcher	Method	St
130	Present Study	2D-Cal	0.171
		3D-Cal	0.173
	Hu (2004)	Exp	0.170
100	Noto and Fujimoto(2006)	2D-Cal	0.168
	Zhang(1995)	2D-Cal	0.173
	Persillon(2001)	3D-Cal	0.164
	Sa and Chang(1990)	2D-Cal	0.157
	Williamson (1996)	Exp	0.204

However as we increase the temperature of the cylinder i.e. when *Ri*>0.19, we see variations in the results from the 2D and 3D calculations. This is represented in Table 8 and Fig. 15.

The results obtained for the heated cylinder case where the *Ri*>0.00, are compared to the results from [15]. As also explained earlier by Hu, when the *Ri*<0.02, the heated cylinder operates in the forced convection regime and the buoyancy effect is negligible. In the discussion for the numerical methodology earlier, we have discussed that all the fluid properties like density, viscosity, thermal conductivity and thermal expansion coefficient varying as a function of the temperature. Based on the same idea, Dumouchel et. al [16] and Wang et al. [17], introduced the concept of effect Reynolds number as a function effective temperature defined as $T_{eff} = T_\infty + 0.28\left(T_w - T_\infty\right)$ which can be used to predict the vortex shedding frequency. However it is already brought to our attention by Hu that this idea is inapplicable to our present study since Dumouchel et. al and Wang et al. have studied the effect of heating only for very small temperature differences ie. Ri<0.02. For small temperature differences the buoyancy effects can be studied using a Boussinesq approximation in the governing equations. This approximation

cannot be implemented for large temperature differences as is the case in the present study.

Table 9. Comparison of St for various Ri

Ri	St (Exp)	St (2D Num)	*St (3D Num)*
0.0	0.171	0.17	0.172
0.19	0.1661	0.162	0.163
0.3	0.152	0.16	0.15
0.5	0.119	0.152	0.127
0.72	0.105	0.142	0.109
1.05	0.1025	0.125	0.1045

The results shown in Table 9 reveal that the 2D simulation for the flow over heated cylinder does not produce accurate results for vortex shedding with Ri>0.3 in comparison to the experimental data [15]. Infact the 2D numerical calculations seem to over predict the vortex shedding frequency for *Ri*>0.3. Whereas the 3D numerical calculations match very close, almost within 2-10 % with the experimental results with the increasing *Ri*. This forms the first step to understanding the possibility of 3D transition being extended for the *Re*=130 and *Ri*>0.02 and we could conclude that 2D numerical simulations are certainly incapable of capturing the flow physics due to the buoyancy effects. For the same reason all the results have been explained only for 3D numerical simulations and not 2D numerical simulations. The 3D transition and its relation to the vortex shedding for higher *Ri* will be more clear from the explanation in the following results.

The difference in the decreasing trend between the experimental data and the numerical results of Chang and Sa [13] has been explained in detail by Hu [15]. For lower Richardson number, Ri=0.31, the vortex shedding pattern in the wake of the heated cylinder is similar to the pattern for the unheated cylinder. However the vortex shedding was found to be delayed and occurs further downstream with the

increasing Ri=0.5. The alternative shedding ceases and the concurrent shedding occurs for Ri>0.71.

Although the numerical simulation by Chang and Sa involved a 2D calculation, it seems to give better agreement with the experimental results than the 2D simulation performed in the present study. Their study used a Boussinesq approximation, although the temperature differences are high, while solving the governing equations. This assumption is not feasible here as explained earlier and is evident in the other results by [13] which cannot predict the buoyancy effect clearly.

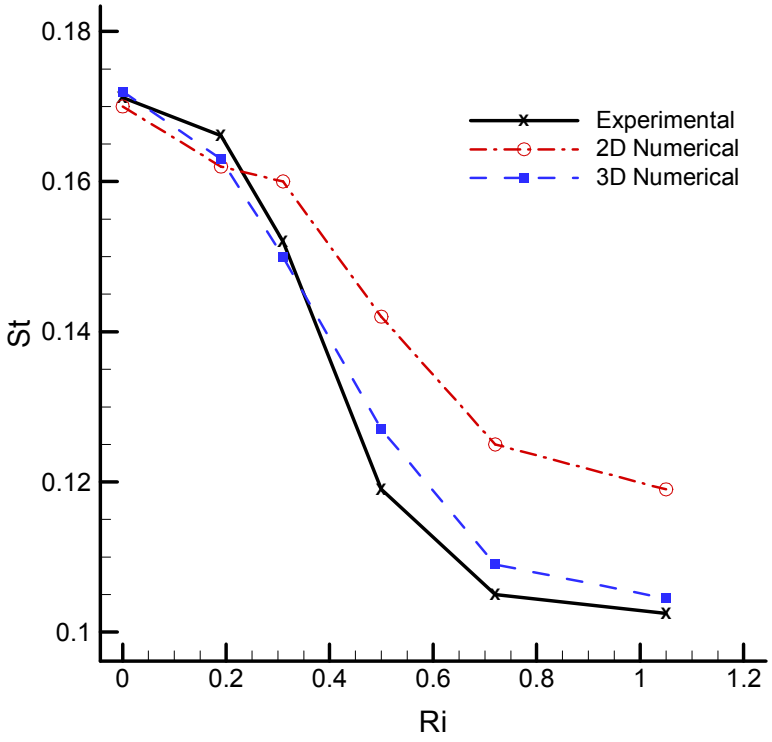

Figure 20. Strouhal Number variation with Richardson Number

3.5 Averaged Nusselt Number

Knowledge of the heat transfer coefficients at low *Re* is invaluable to designers and engineers. In this section we will focus on the averaged Nusselt number, *Nu*. In Eqn. 3.2 $\overline{Nu}$ is the averaged Nusselt number and $\overline{Q}$ is the averaged heat transfer rate.

$$\overline{Nu} = \frac{hD}{k} = \frac{\overline{Q}D}{A^2 k(T_w - T_\infty)}$$

Different studies and understanding of this aspect has been discussed by Hu. In this case we have a mixed convection resulting from the heat transfer by forced and free convection. The experimental data by Hu suggests that with the increasing Ri, $\overline{Nu}$ decreases [15]. Figure 21, shows the comparison of the results obtained from the present numerical study with the experimental results of Hu.

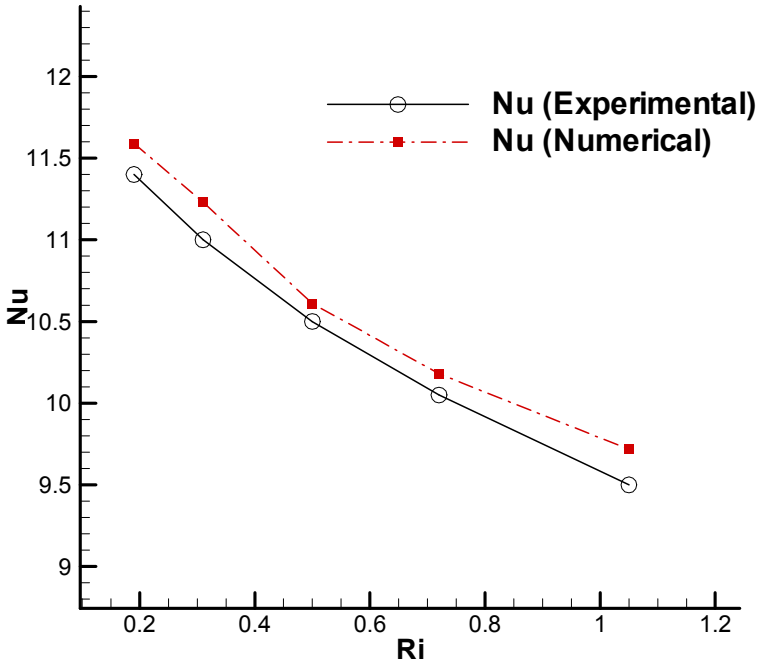

Figure 21. Variation of averaged Nusselt number with Ri.

The numerical results indicate the same trend as the experimental results, though they seem to over predict the $\overline{Nu}$ by around 10%. But the results clearly indicate that with the increasing Ri the effect of buoyancy increases. The forced convection and free convection are in opposite direction and are added vectorally which results in the decreasing trend.

3.6 Thermal effect of buoyancy on 3D wake flow

For flows with small AR (less than 28) or finite length of cylinders, we would see a 3D transition of wake behavior different from that for the cylinders with infinite length or large aspect ratio, AR. From the studies by Williamson [3], for the unheated cylinders with large AR the transition regime would be between 190<Re<250. However this transition regime is extended and/or delayed for a cylinder with small AR with “no-slip” walls [6]. This suggests that besides Re, the end-effects and AR plays a significant role in the nature of the flow behind a cylinder.

In the present study, the cylinder with a small AR = 7 has been considered. In addition to this, a no-slip boundary condition has been implemented for the walls. These factors significantly affect the wake behavior of the flow although the Re=130 does not lie in the usual transition regime of 190-250. Instead we see a 3D wake behavior for flow at this Re which is also depicted in various results compared above.

Besides this, it is also interesting to see the influence of heat input on the 3D wake flow characteristics. There have been previous studies conducted by Steenhoven, to study the thermal effects on the wake of a cylinder in cross flow arrangement and its influence on the 3D transition of the flow [18]. Their results indicate that heating would result in mixed convection resulting in an early 3D transition (mode E) of the flow for *Ri*=0.35-1.50 as shown in Fig. 2. The non-

parallelism between the cross flow (streamwise) direction and the buoyant force causes the flow to become asymmetric. This also results in different characteristics of the upper and lower row of the vortices.

However in the current study the flow is in the direction of gravity and opposing the buoyant force. We have already discussed the influence of heat input and buoyancy on the wake behavior in terms of the vortex shedding frequency, time-averaged centerline velocities, time-averaged drag coefficient and Nusselt number. We have also mentioned that all these results are also influenced significantly by the end conditions which lead to 3D wake behavior.

Figure 22-28 show the instantaneous pressure, velocity components and vorticity components for the temporally periodic flow for Ri=0.0 when the cylinder is not heated. We are looking at the yz section passing through the axis of the cylinder. We can observe the spatial development of the boundary layer at the wall due to the no-slip boundary condition and we do not observe vortex shedding here due to the presence of the boundary layer.

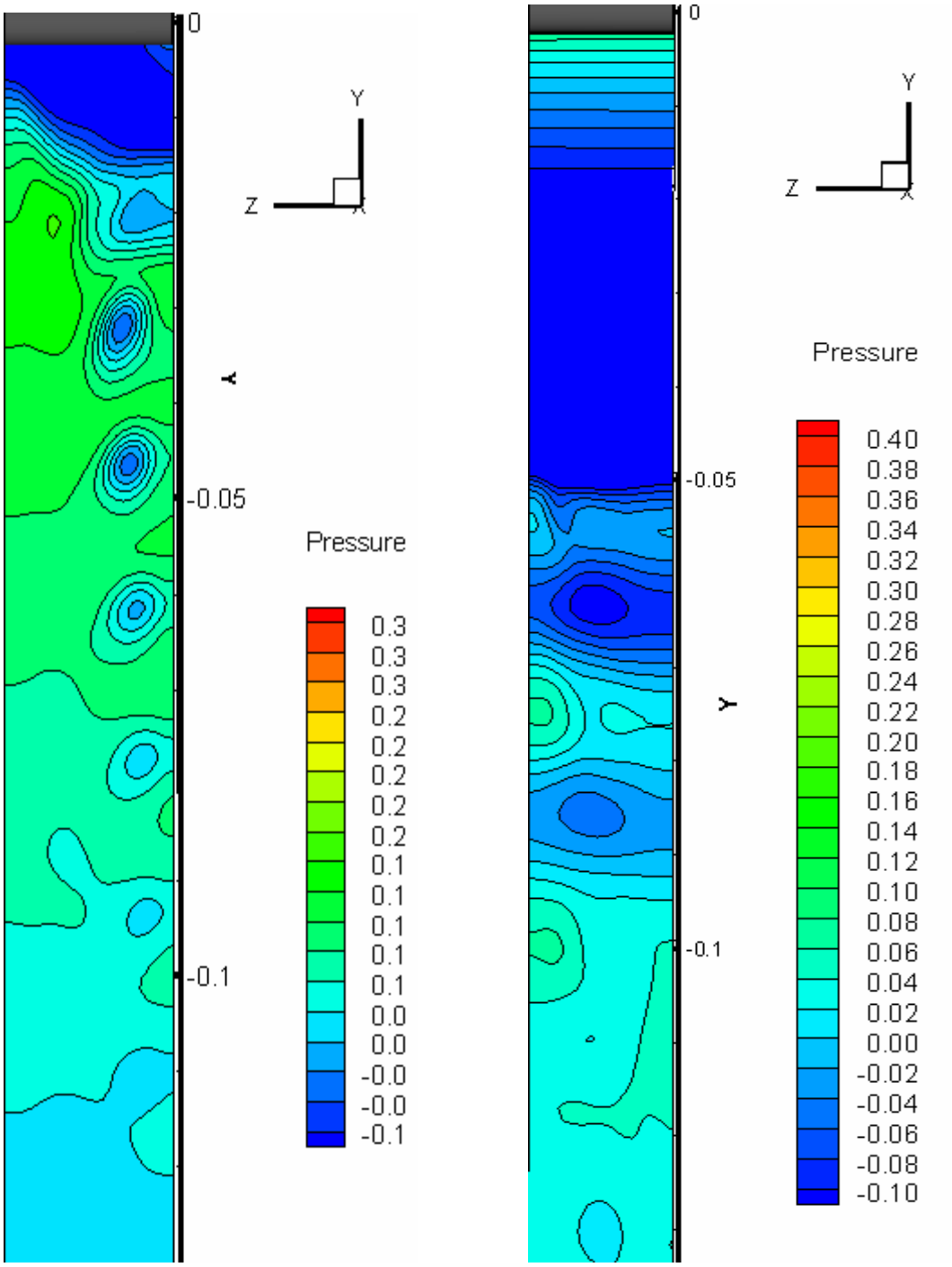

(a) **(b)**

Figure 22. Instantaneous pressure contours (a) Ri=0.0 (b) 1.05

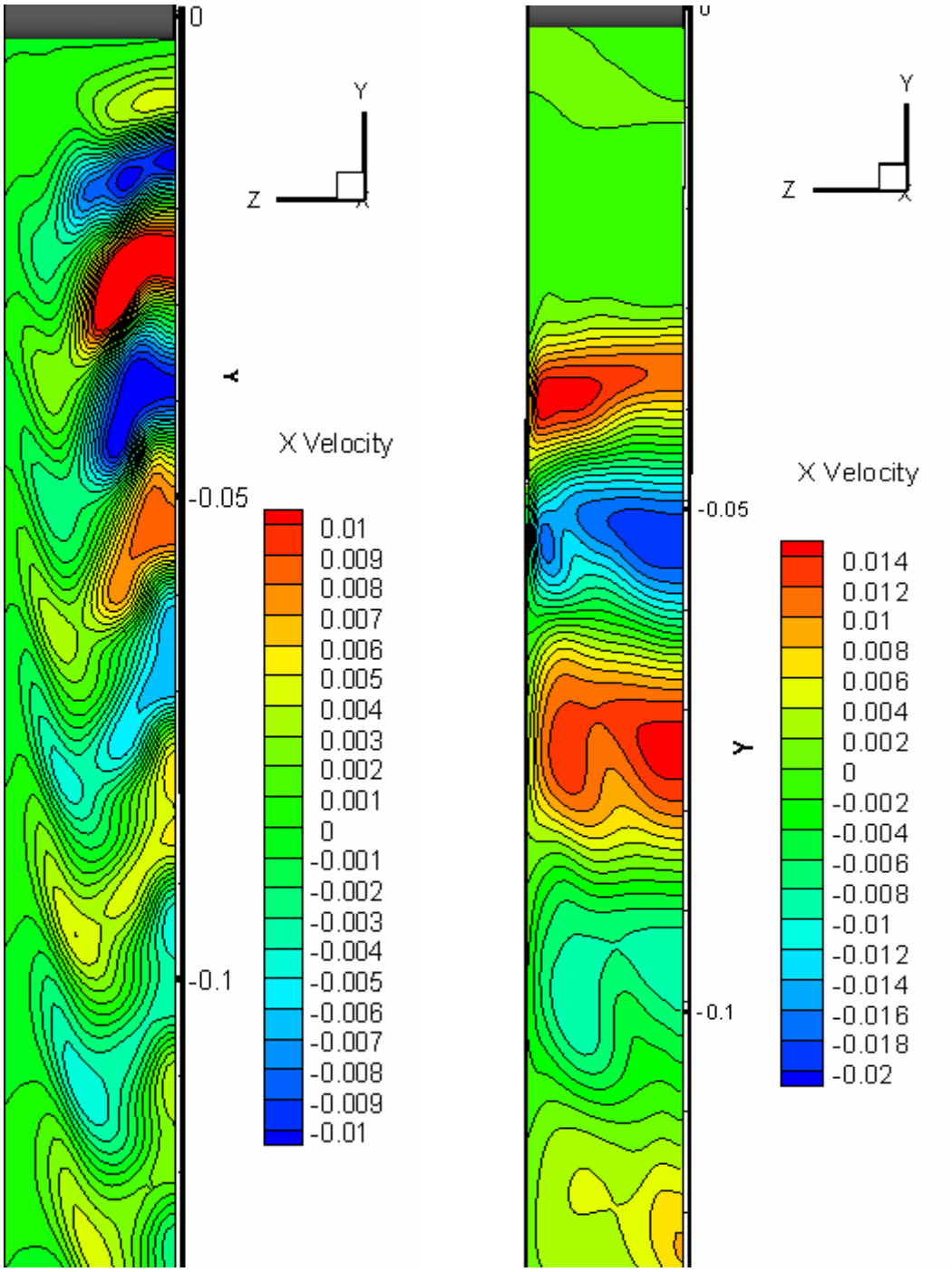

(a) **(b)**

Figure 23. Instantaneous x-velocity component (a) Ri=0.0 (b) 1.05

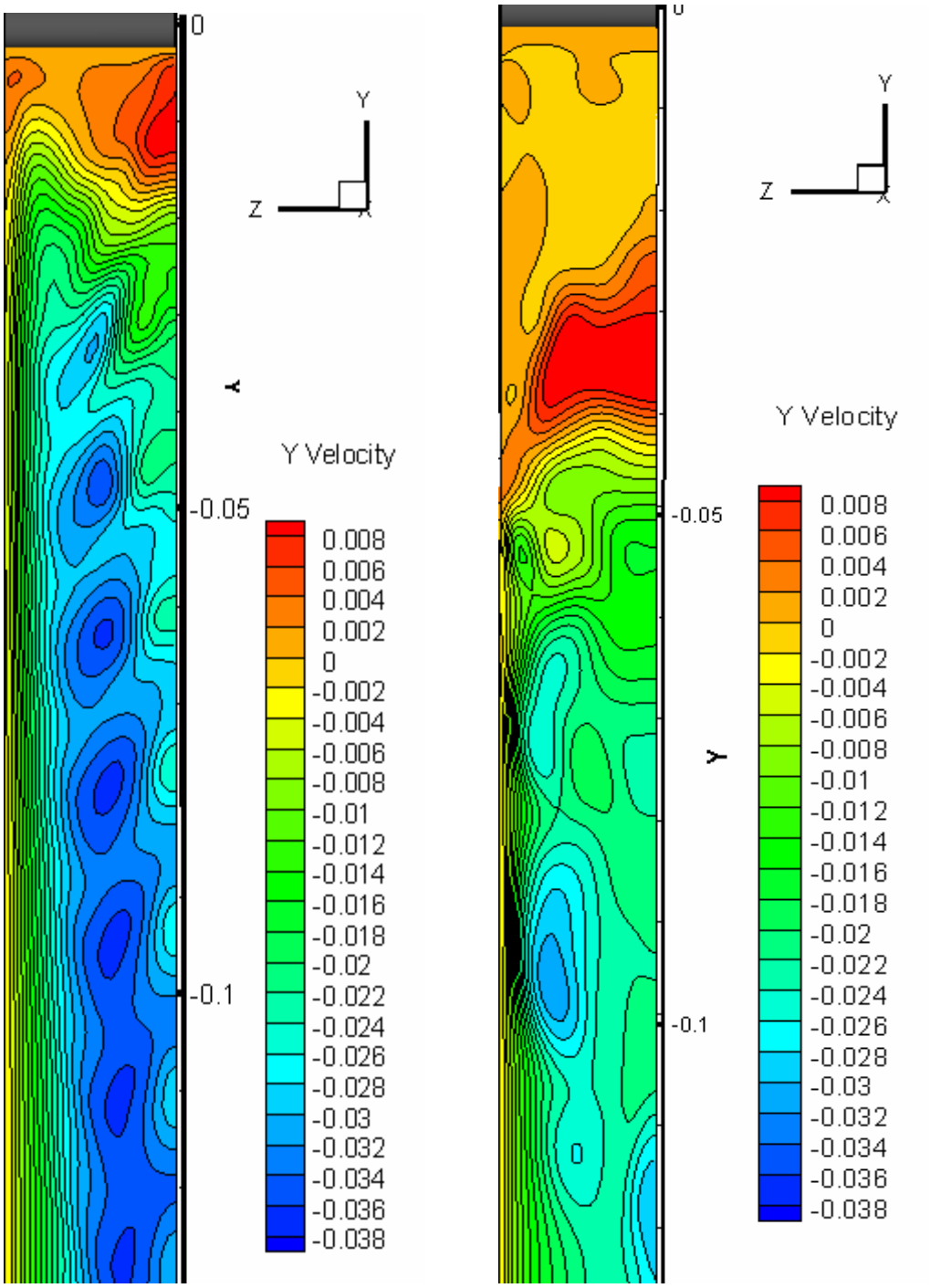

(a) **(b)**

Figure 24. Instantaneous y-velocity component (a) Ri=0.0 (b) 1.05

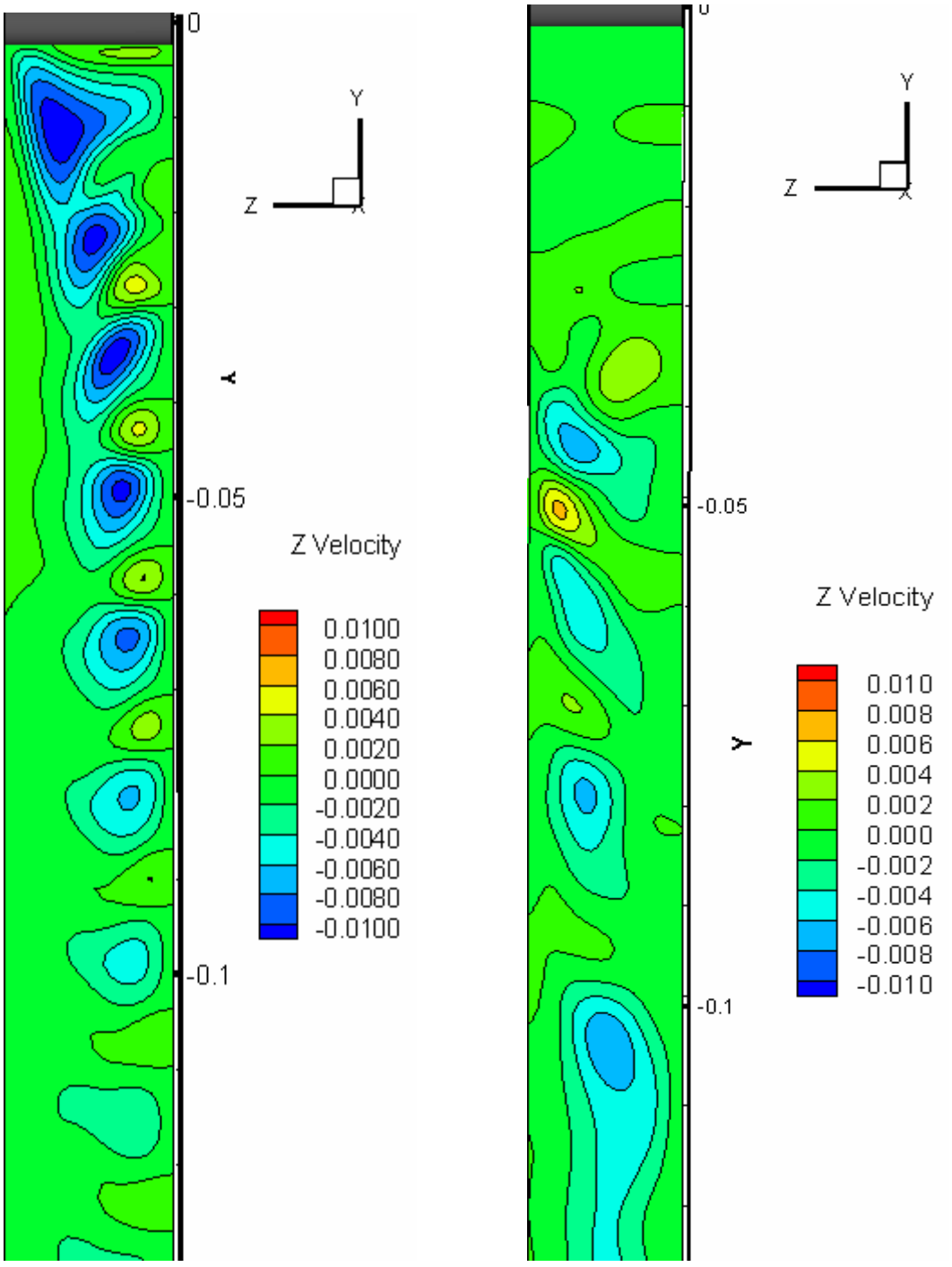

(a) **(b)**

Figure 25. Instantaneous z-velocity component (a) Ri=0.0 (b) 1.05

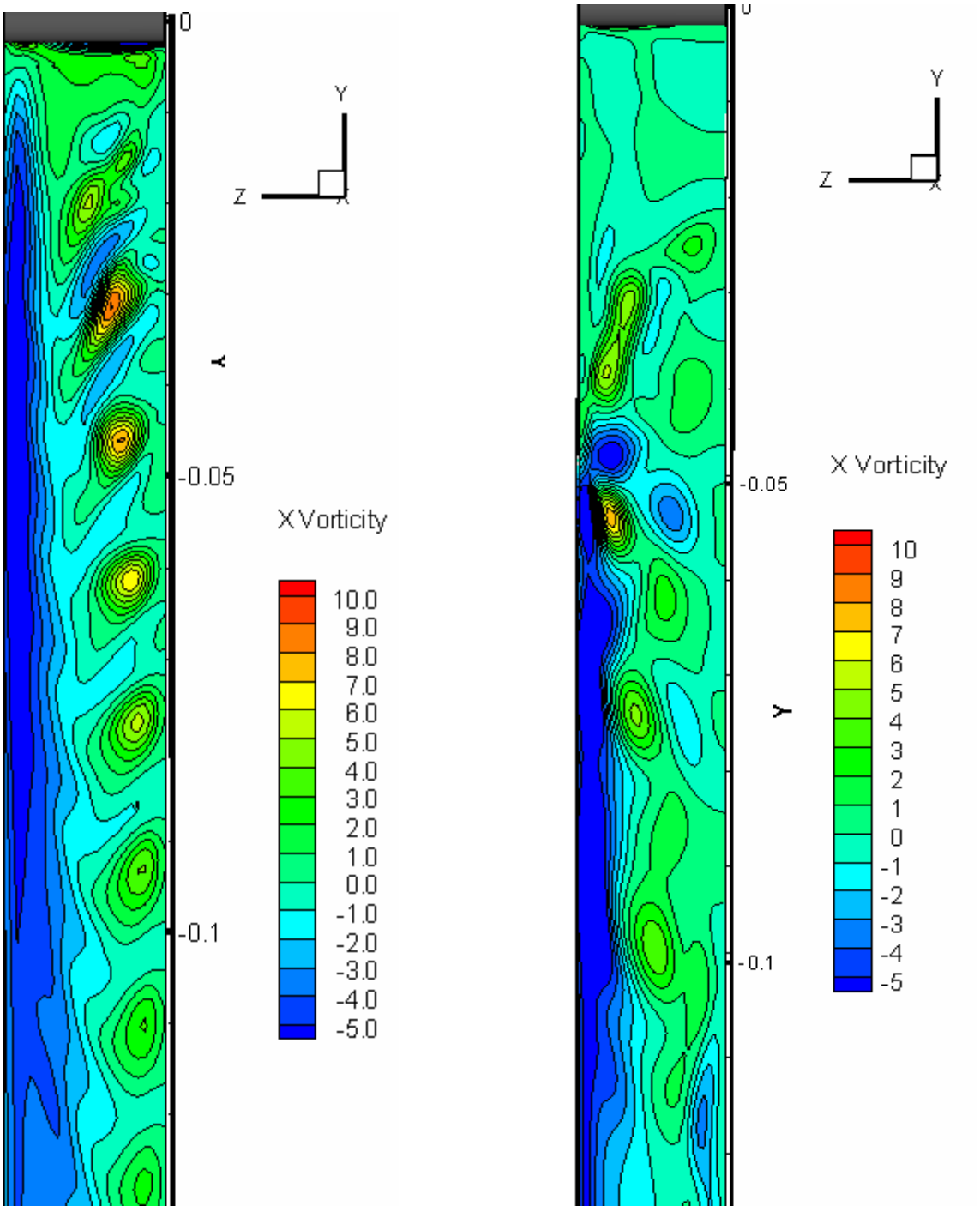

(a) **(b)**

Figure 26. Instantaneous x-vorticity component (a) Ri=0.0 (b) 1.05

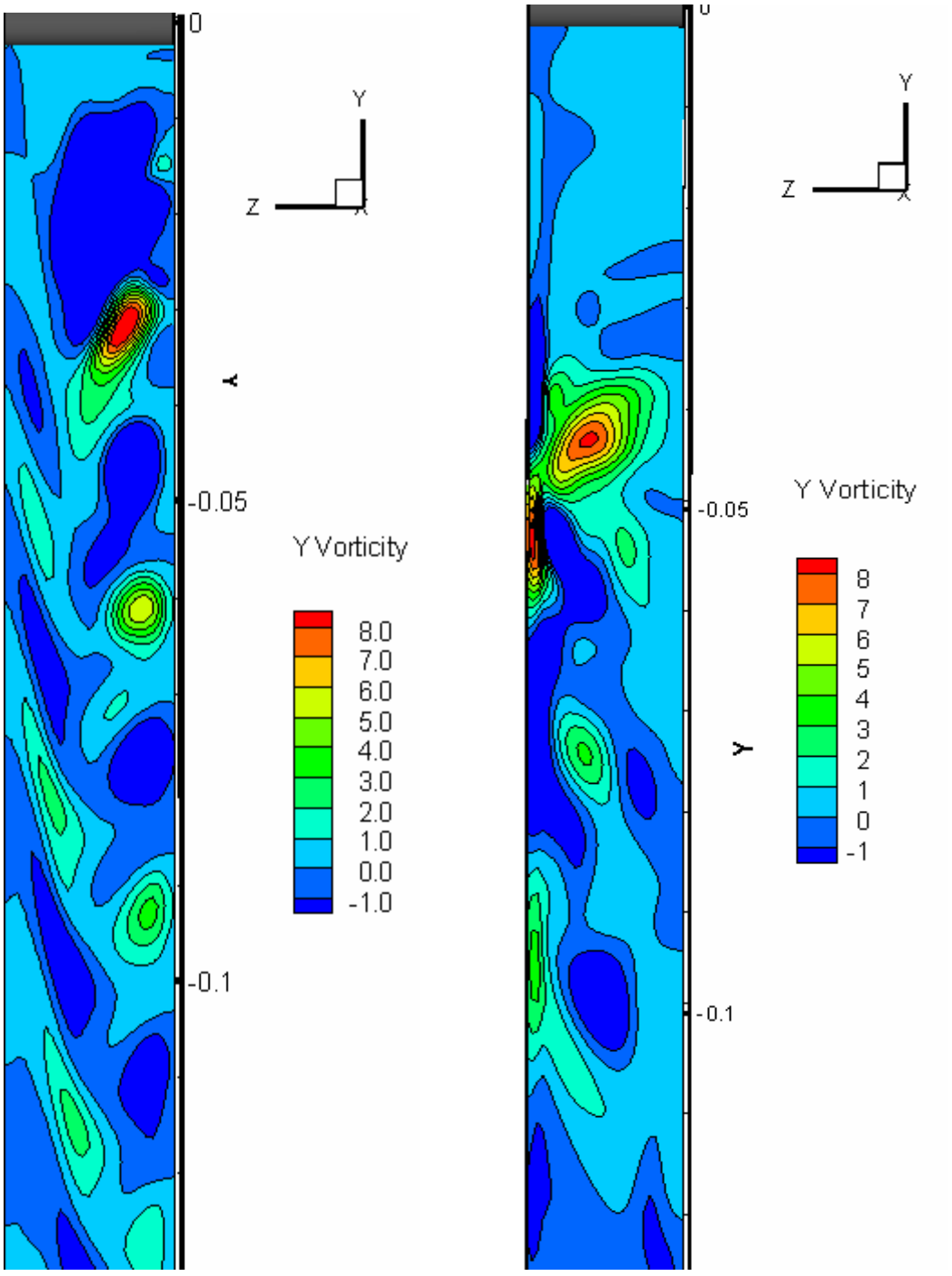

(a) **(b)**

Figure 27. Instantaneous y-vorticity component (a) Ri=0.0 (b) 1.05

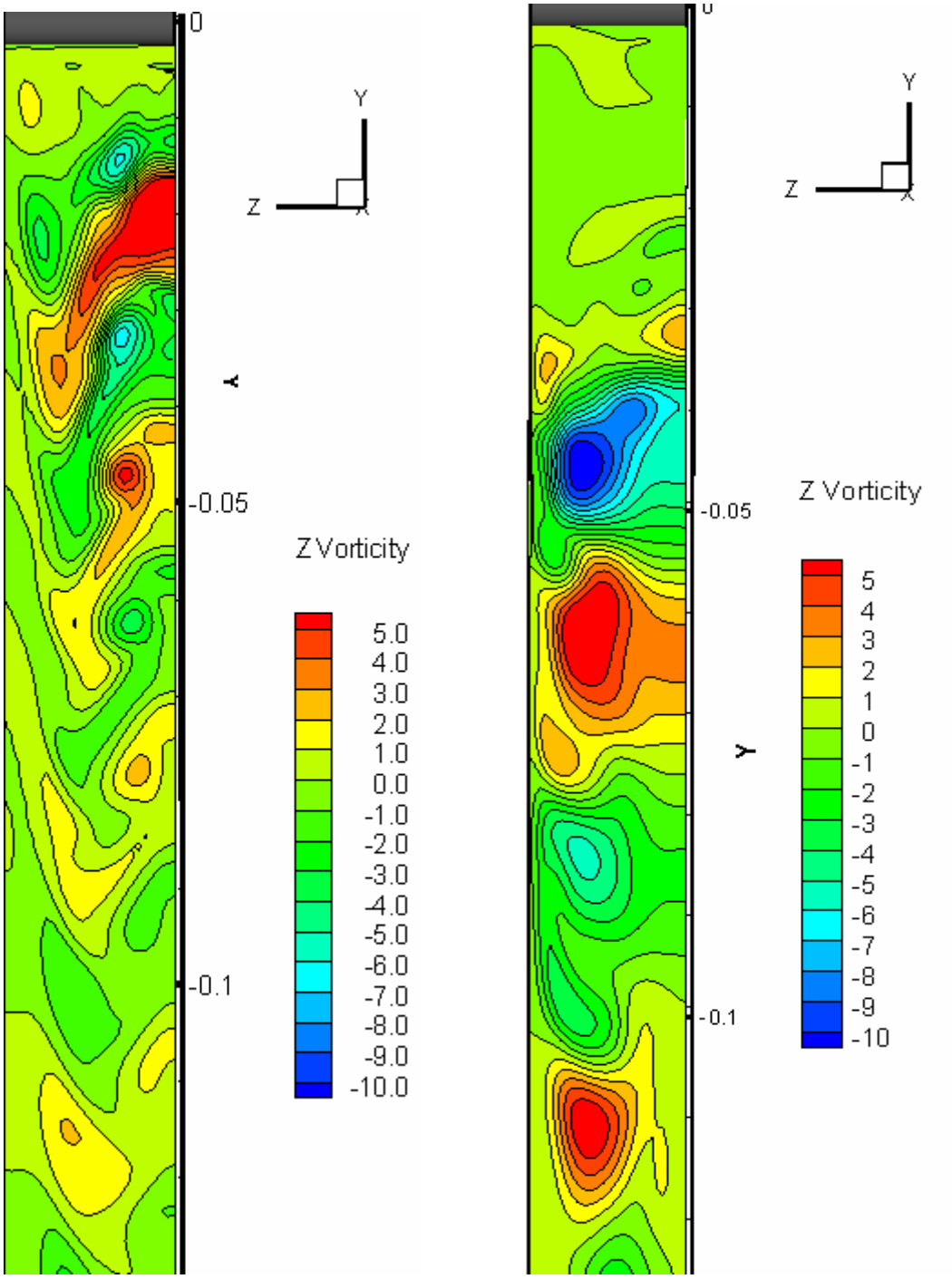

(a) **(b)**

Figure 28. Instantaneous z-vorticity component (a)Ri=0.0 (b)1.05

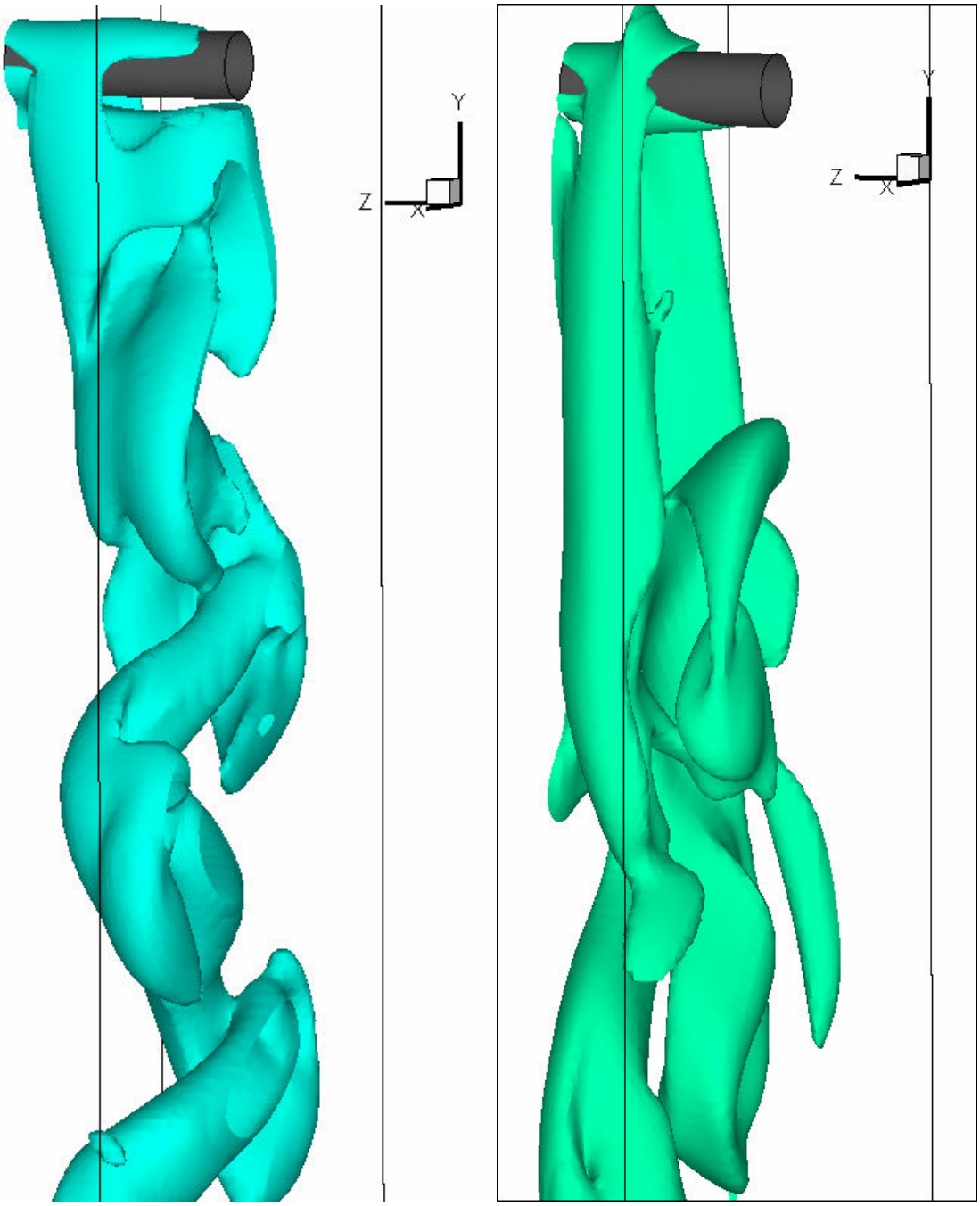

(a) **(b)**

Figure 29. Iso-surface for x-vorticity =0.5 (a)Ri=0.0 (b) 1.05

The transition to the three-dimensionality in the wake can be conveniently illustrated using the relationship between the *St* and *Re*. In the Fig. 1 [3] the first discontinuity of the Strouhal frequency occurs at Re at 180-190(mode A). The wake

in this mode is associated with vortex loops and formation of streamwise vortex pairs due to the formation of primary vortices. The wavelength of the vortex deformations is 3-4 cylinder diameters. With the increasing *Re* from 230-260, we see another discontinuity (mode B) with the wavelength of streamwise vortex structures as one cylinder diameter approximately.

During the transition, the time histories of the lift forces are associated with two peaks: a peak at lower frequency that corresponds to mode A that gradually diminishes and a peak at higher frequency that takes over as the Re increases. Williamson [3] attributes this to the intermittent swapping between the two modes. A similar trend is observed for *Ri*=1.05 shown in Fig. 30 and Fig. 31. The temporal history of lift force shows two different modes. One of the modes diminishes with time and the other one becomes dominant. Thus we observe a low and high frequency in Fig. 30.

Figures 22 to 28 show the instantaneous pressure, velocity components and vorticity components for *Ri*=1.05 at yz plane. It is clear that the wake becomes very unstable because of the heating. This would suggest that heating and small aspect ratio would prolong or delay onset of transition regime. In this case, the transition that would start in *Re* range 190-250 seems to start earlier because of heating. However more work is needed to understand the effect of heating and small aspect ratios on transition. The details study of the vortex patterns and wake instability would aid in the understanding of the same. In addition to this, a large number of *Ri* would give more insight into this phenomenon.

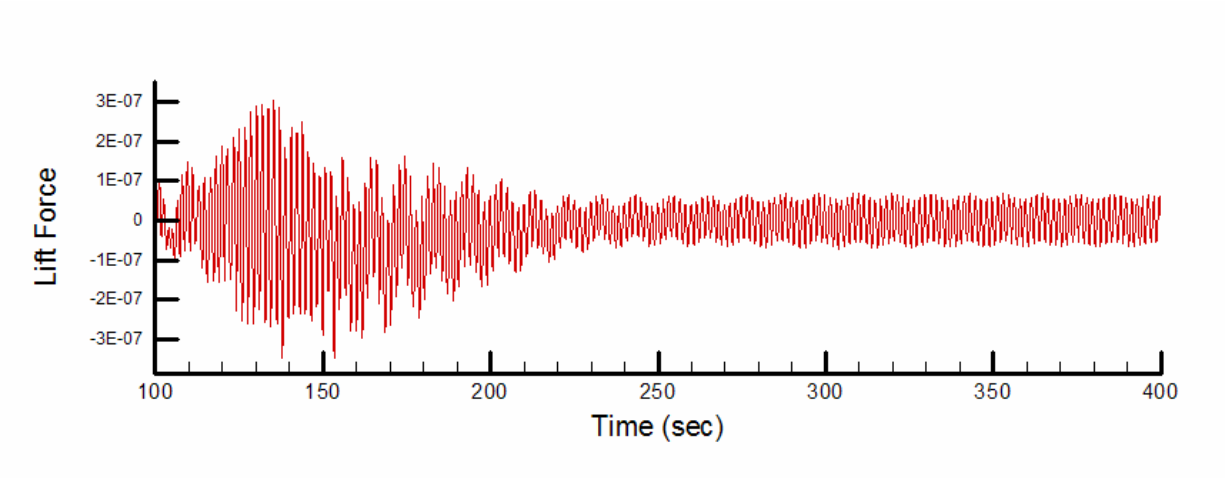

Figure 30. Temporal history of lift force for Ri=1.05

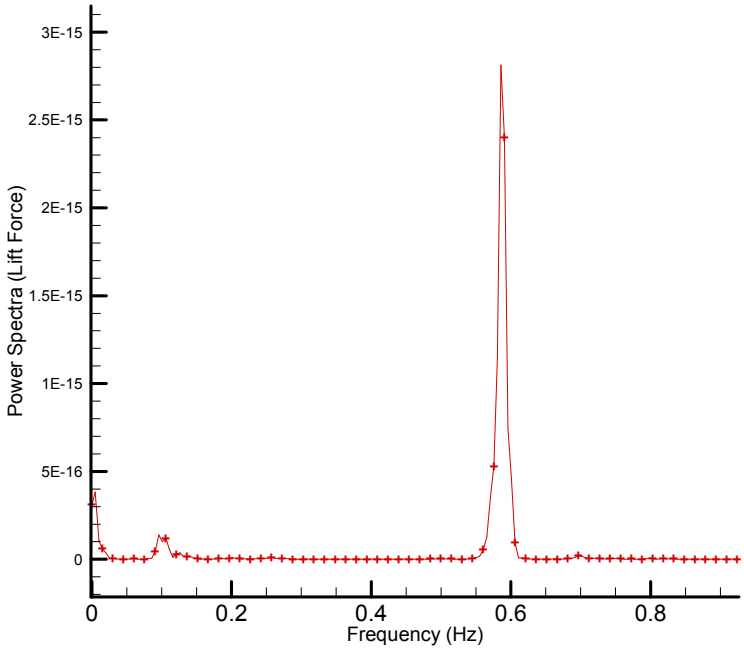

Figure 31. Power spectra of lift force time history Ri=1.05

CHAPTER 4. CONCLUDING REMARKS

The influence of buoyancy opposing the flow direction due to mixed convection is numerically simulated for flow past a circular cylinder with small aspect ratio (*AR*=7) at *Re*=130. The Richardson number based on the temperature of the cylinder varies between *Ri*=0.0 to 1.05. Numerical results are generated with time-accurate finite volume method based unsteady compressible Navier-Stokes equations. The implementation of the boundary conditions and physical properties are based on the experimental set up conditions. Most of the previous studies have been conducted with the slip boundary conditions. In the present study the influence of heating in addition to small aspect ratio of the cylinder and no-slip wall boundary conditions on the pressure distribution, time-averaged drag co-efficient, time-averaged centerline velocities, Strouhal number, averaged Nusselt number and transition mechanism has been numerically investigated and validated with the available experimental results. Some of the broad conclusions can be outlined as follows:

1. Due to the small aspect ratio with no-slip walls, we see a 3D wake for *Re*=130 unlike the large aspect ratio. Under the influence of buoyancy the flow separation occurs earlier than when the cylinder is not heated. This results in a wider and longer wake for the heated cylinder and a narrower wake for the unheated cylinder.
2. The wake closure length increases with the Richardson number and consequently the averaged drag coefficient is higher for the heated cylinder. The drag has a significant contribution from the pressure drop whereas the drag due to skin friction is negligible.

3. The vortex shedding frequency in terms of Strouhal number almost approaches zero with the increasing Richardson. This suggests that heating suppresses the vortex shedding frequency.
4. Averaged Nusselt number follows the same decreasing trend as the experimental results with the increasing Richardson number.
5. Preliminary analysis for influence of buoyancy on the wake behavior at Re=130 for cylinder in contra flow suggests that heating instigates an early transition. It is interesting to observe the significance of small aspect ratio and end effects in addition to the heating, on the transition mechanism. However much more work needs to be done over a larger range of temperature and Reynolds number to determine the onset of transition before any certain conclusions can be drawn.
6. Detailed analysis of the vortex shedding patterns and vortex dislocations can aid in the understanding of various modes in transition regime for a heated cylinder.

REFERENCES

[1] Berger, E., and Wille, R., “Periodic Flow Phenomena,” *Annual Review of Fluid Mechanics*, Vol. 4, 1972, pp. 313-340.

[2] Williamson, C. H. K., “Defining a universal and continuous Strouhal relationship for the laminar vortex shedding of a circular cylinder,” *Physics of Fluids*, Vol. 31, No. 10, 1988, pp. 2742-2744

[3] Williamson, C. H. K., “Vortex Dynamics in the Cylinder Wake,” *Annual Review of Fluid Mechanics*, Vol. 28, 1996, pp. 477-526.

[4] Mittal, R., and Balachandar, S., ‘‘Effect of three-dimensionality on the lift and drag of nominally two-dimensional cylinders,’’ *Physics of Fluids*, Vol. 7, No. 8, 1995, pp. 1841-1865.

[5] Ren, M., Rindt C. C. M., and Steenhoven A. A. V., “Experimental and numerical investigation of the vortex formation process behind a heated cylinder,” *Physics of Fluids*, Vol. 16, No. 8, 2004, pp. 3103-3114

[6] Mittal, S., “Computation of three-dimensional flows past circular cylinder of low aspect ratio,” *Physics of Fluids*, Vol. 13, No. 1, 2001, pp177-191.

[7] Eaton, B.E., “Analysis of laminar vortex shedding behind a circular cylinder by computer-aided flow visualization,” *Journal of Fluid Mechanics*, Vol. 180, 1987, pp117-145.

[8] Hatton, A. P., James, D. D., and Swire, H. W., “Combined Forced and Nature Convection with Low Speed Air Flow over Horizontal Cylinders,” *Journal of Fluid Mechanics*, Vol. 42, 1970, pp17-31.

[9] Ooesthuizen, P.H., and Madan, S., “Combined convective heat transfer from horizontal circular cylinders in air,” *Transactions of ASME Journal of Heat Transfer*, Vol. 92, 1970, pp. 194-196.

[10] Jain, P.C., and Lohar, B.L., “Unsteady mixed convection heat transfer from a horizontal circular cylinder,” *Transactions of ASME Journal of Heat Transfer*, Vol. 101, 1979, pp. 126-131.

[11] Noto, K., and Matsumoto, M., “Generation and suppression of the Karman vortex street upon controlling surface temperature of a cylinder,” *Proceedings of Numerical Methods Laminar and Turbulent Flows*, Vol. 7, 1991, pp. 671-678.

[12] Badr, H.M., “Laminar combined convection from a horizontal cylinder in parallel and contra flow regimes,” *International Journal of Heat and Mass Transfer*, Vol. 27, No. 1, 1984, pp. 15-27.

[13] Chang, K.S. and Sa, J.Y., “The effect of buoyancy on vortex shedding in the near wake of a circular cylinder,” *Journal of Fluid Mechanics*, Vol. 220, 1990, pp. 253-260.

[14] Steenhoven A. A. V., and Rindt, C. C. M., “Flow Transition Behind a Heated Cylinder,” *International Journal of Heat and Fluid Flow*, Vol. 24, 2003, pp 322-333.

[15] Hu, H., and Kochesfahani, M., “The Wake Behavior behind a Heated Cylinder in Forced and Mixed Convection Regimes,” *ASME Summer Heat Transfer Conference,* San Francisco, CA, USA. Jul, 2005.

[16] Dumouchel, F., Lecordier, J. C., and Paranthon, P. P., “The Effective Reynolds Number of a Heated Cylinder”, *International Journal of Heat and Mass Transfer*, Vol. 40, No. 12, 1998, pp. 1787-1794.

[17] Wang, A., Travnick, Z., and Chia, K., “On the Relationship of Effective Reynolds Number and Strouhal Number for the Laminar Vortex Shedding of a Heated Circular Cylinder,” *Physics of Fluids*, Vol. 12, No. 6, 2000, pp. 1401-1410.

[18] Kieft, R. N., Rindt, C. C. M., and Steenhoven, A. A. V., “The Wake Behavior Behind a Heated Horizontal Cylinder,” *Experiments in Thermal and Fluid Science*, Vol. 19, No.4, 1999, pp. 183-193.

[19] Sharma, G.K., and Sukhatme, S.P., “Combined free and forced convection heat transfer from a heated tube to a transverse air stream,” *Transactions of ASME Journal of Heat Transfer*, Vol. 91, 1969, pp. 457-459.

[20] Hatanaka, K., and Kawahara, M., “Numerical study of vortex shedding around a heated/cooled circular cylinder by the three step Taylor-Galerkin method,” *International national Journal for Numerical Methods in Fluids*, Vol. 17, 1993, pp. 349-364.

[21] Joshi, N. D., and Sukhatme, S. P., “An analysis of combined free and forced convection heat transfer from a horizontal circular cylinder to a transverse flow,” *Transactions of ASME Journal of Heat Transfer*, Vol. 92, 1970, pp. 194-196.

[22] Sparrow, E. M., and Lee, L., “Analysis of a mixed convection about a horizontal cylinder,” *International Journal of Heat and Mass Transfer*, Vol. 19, 1976, pp. 229-231.

[23] Merkin, J. H., “Mixed convection from a horizontal circular cylinder,” *International Journal and Mass Transfer*, Vol. 18, 1977, pp. 73-77.

[24] Patnaik, B. S. V. P., Seetharamu, K.N., and Narayana, A. P. A., “Simulation of laminar confined flow past a circular cylinder with integral wake splitters involving heat transfer,” *International Journal of Numerical Methods for Heat and Fluid Flow*, Vol. 6, No. 4, 1996, pp. 65-81.

[25] Gowda, Y.T.K., Patnaik, B. S. V. P., Seetharamu, K.N., and Narayana, A. P. A., “Finite element simulation of transient laminar flow and heat transfer

past an in-line tube bank," *Journal of Heat and Fluid Flow*, Vol. 19, No. 1, 1998, pp. 49-55.

[26] Ren, G., and Utnes, T., "A Finite element solution of time-dependent incompressible Navier-Stokes equations using a modified velocity correction method," *International Journal for Numerical Methods in Fluids*, Vol. 17, 1993, pp. 349-364.

[27] Chorin, A.J., "Numerical simulations of Navier-Stokes equations," *Mathematical Computations*, Vol. 22, 1968, pp. 745-762.

[28] Patnaik, B.S.V., "Finite element analysis of flow past a circular cylinder and two cylinders in tandem: influence of vibration, buoyancy," Ph.D. Dissertation, Indian Institute of Technology, Madras, India, 1998.

[29] Grift, O.M., Votaw, C. W., "The vortex street in the wake of a vibrating cylinder," *Journal of Fluid Mechanics*, Vol. 51, No. 1, 1972, pp. 31-48.

[30] Chilukuri, R., "Incompressible laminar Flow past a transversely vibrating cylinder," *Transactions of ASME Journal of Fluids Engineering*, Vol. 109, 1987, pp. 166-171.

[31] Karniadakis, G.M., "Numerical simulation of forced convection heat transfer from a cylinder in cross flow," *International Journal of Heat and Mass Transfer*, Vol. 31, No. 1, 1988, pp. 107-118.

[32] Kovasznay, L.S.G., "Hot wire investigation of the wake behind cylinders at low Reynolds numbers," *Proceedings of the Royal Society*, Series A, Vol. 198, 1949, pp. 174-190.

[33] Chun, W., and Boehm, R. F., "Calculation of forced Flow and heat transfer around a circular cylinder," *Numerical Heat Transfer*, Vol. 15, 1989, pp. 101-122.

[34] Dennis, S.C.R., and Chang, G.Z., “Numerical solution of steady flow past a circular cylinder at Reynolds numbers up to 100,” *Journal of Fluid Mechanics*, Vol. 42, 1970, pp. 471-489.

[35] Fluent Notes and User Manual (2003)